

A Hybrid Numerical-Asymptotic Boundary Element Method for High-Frequency Wave Scattering



Emile PAROLIN

Keble College

University of Oxford

A thesis submitted for the degree of
*Master of Science in Mathematical Modelling
and Scientific Computing*

2015

Acknowledgements

I sincerely thank my supervisor Dr David HEWETT for his guidance, support and interest throughout this project work. His expertise and invaluable advice at every stage helped me carry out a work on a topic that was of great interest to me and a constant source of motivation. His enthusiasm made it a pleasure to work with him.

I would like to thank Dr Stephen LANGDON from the University of Reading for making available MATLAB routines to compute oscillatory integrals using a Filon-type method. I thank also Mikael SLEVINSKI for his kind help and advice on the use of the `SingularIntegralEquation.jl` JULIA package.

I am also grateful to Dr Kathryn GILLOW and all the professors during this M.Sc. course. Their lectures provided me with the theoretical and methodological background that aroused my interest for this topic and helped make this year unique and challenging.

Abstract

We present a hybrid numerical-asymptotic (HNA) hp boundary element method for solving the problem of time-harmonic scattering of an incident plane wave by two-dimensional planar screens with sound-soft (Dirichlet) boundary conditions. The method uses a HNA approximation space enriched by oscillatory basis functions chosen to efficiently capture the high-frequency asymptotics of the solution. Previous work using this approach for scattering problems is essentially conducted using Galerkin schemes. In this work, we investigate via numerical experiments a related collocation method, for which we demonstrate that similar convergence rates are achieved. The performance of the method is characterised by a computational cost almost frequency independent, providing that appropriate highly oscillatory numerical quadrature is implemented.

Contents

1	Introduction	1
2	Boundary integral equation	4
2.1	Wave scattering problem	4
2.2	Boundary Integral Equation	5
2.3	High-Frequency Asymptotics	7
3	Numerical method	10
3.1	Hybrid Numerical-Asymptotic approximation space	10
3.2	Collocation method	15
3.3	Allocation of the collocation points	17
4	Numerical quadrature	19
4.1	Integral evaluation required by the method	19
4.2	Gauss-Legendre quadrature	20
4.3	Highly oscillatory quadrature	21
4.4	Treatment of singularities	23
4.5	Calibration of the numerical quadrature routines	24
5	Numerical results	29
5.1	Comparison of the different approximation strategies	29
5.2	A more challenging test case	42
5.3	Execution time	49
6	Conclusions	51
	Bibliography	52

Chapter 1

Introduction

We present a numerical method for solving two-dimensional high-frequency wave scattering problems. Scattering problems arise in numerous areas of science and engineering such as acoustics, electromagnetics or linear elasticity. These problems are usually stated as boundary value problems, involving a partial differential equation for the unknown wave field u and appropriate boundary conditions on the scatterer boundary Γ . If the medium of propagation of the wave is homogeneous, the partial differential equation can take the simple form of the Helmholtz equation, $(\Delta + k^2)u = 0$, for a wave number $k > 0$.

Wave scattering problems can be solved with classical finite element methods (FEM) for instance. However, problems are often posed on unbounded domains (exterior problems) which imposes to truncate the domain and implement an absorbing boundary condition on the fictive boundary, such as a 'perfectly matched layer'. An attractive alternative approach is to recast the problem on the boundary of the domain, the scatterer, using for instance Green's theorem. This is possible thanks to the availability of a fundamental solution of the partial differential equation. A boundary integral equation (BIE) is then obtained, the global nature of which is the price to pay for reducing the dimension by one. This second approach is the basis of the boundary element methods (BEM) considered here.

Different numerical approaches are possible to solve the BIE, among which the Galerkin and collocation methods¹. In both methods one starts by considering a finite-dimensional approximation space in which to look for a solution. The difference between the two approaches is the way they numerically select a member of the approximation space considered. The Galerkin scheme is based on a variational

¹Other methods include the quallocation method of Sloan [30] or the Nyström method [25] also referred to as the quadrature method.

reformulation of the integral equation whereas the collocation approach imposes the BIE to hold exactly at a finite set of points on the boundary. The conventional choice for the approximation space is to use a space of piecewise polynomial functions. Such a choice implies that the number of degrees of freedom used by the method grows at least linearly with the wave number k in order to capture the increasing oscillations of the solution. In this context, any numerical method is impractical at high frequency and one must turn to asymptotic methods. However, asymptotic approximations are only arbitrary accurate as the wave number k tends to infinity. There is therefore a gap between moderate and very large frequencies for which no efficient numerical method can provide solutions at an arbitrary precision.

To overcome such limitations, a key idea that has been proposed is to introduce into the approximation space some known asymptotic behaviour of the solution at high frequencies, in an attempt to reduce the number of degrees of freedom required at large frequencies. FEM and BEM schemes that incorporate some asymptotic knowledge into the approximation space are referred to as hybrid numerical-asymptotic (HNA) methods, and have been the subject of recent research, reviewed in [8]. Most of the asymptotics built in the approximation space are known from the geometrical theory of diffraction (GTD); see [5]. From the knowledge of the GTD it is in particular possible to enrich the piecewise polynomial approximation space with oscillatory basis functions, leaving only the amplitude of the oscillations to be approximated numerically by piecewise polynomial functions.

The HNA methods are well suited to problems where the high-frequency asymptotics are relatively simple in order to be inserted into the approximation space with moderate complexity. It has been applied mainly in the context of BEMs, which require only the knowledge of the asymptotic behaviour of the solution on the scatterer (unlike FEM), and to two-dimensional (2D) problems. The 2D problems that have been currently investigated include scattering by sound-soft smooth convex obstacles [3, 32], convex [2, 11, 17] and non-convex polygons [10], and planar screens [16]. With the exception of [2], the HNA approach is conducted in these works within a Galerkin framework and has proved to be very effective in reducing the number of degrees of freedom required at large frequencies. The theoretical analysis of the method is also greatly covered and convergence proofs are available. Such variational methods are however rather difficult to implement as they require the evaluation of two-dimensional oscillatory integrals. In the prospect of generalisation of the method to higher dimensions, for which the implementations of such Galerkin

schemes would become rather difficult, alternative approaches are considered. In particular, an attractive alternative comes from collocation schemes, which only requires the evaluation of one-dimensional oscillatory integrals. This is the approach considered in [2] for instance, where a BEM scheme is developed for convex polygons in 2D. The BEM described is an h -version in which the HNA approximation space uses piecewise constant functions to approximate the amplitudes of the oscillations. Other research in the context of the scattering problems considered here and using a collocation method, although with no particular attention to the high frequency case, have proved to be very successful, see [4, 7, 13, 14]. In the present work, we propose to extend the HNA collocation approach of [2] to an hp -version of the BEM method and work on the problem of the scattering by planar screens in 2D as in [16]. The main goal is to experimentally investigate the performance of the method, in particular by studying how the design of the HNA approximation space and the distribution of the collocation points on the boundary affect accuracy and conditioning.

An outline of this work is as follows. In Chapter 2, we first describe in Section 2.1 the problem of the scattering by sound-soft planar screens which is considered here. This involves writing the boundary value problem with the Helmholtz equation and the associated boundary conditions. In Section 2.2 we reformulate the problem as a boundary integral equation, which is the equation we are aiming to solve using a BEM. We then continue in Section 2.3 by specifying the high-frequency asymptotic form of the solution and on which the approximation space is built. Chapter 3 is then dedicated to the description of the numerical method. Precisely, we define in Section 3.1 the HNA approximation space considered, before explaining how we propose to numerically select members of this approximation space by using a collocation method in Section 3.2. Chapter 3 ends with Section 3.3 which presents the different distributions of collocation points that we consider. The numerical quadrature strategy, which is an essential ingredient in the method, is then introduced and discussed in Chapter 4. The numerical integration required is carried out using appropriate oscillatory integration routines so that the method has a frequency-independent computational cost. In particular, the Filon-type highly oscillatory quadrature rule used is described in Section 4.3. The results of our numerical experiments are presented in Chapter 5. The efficiency of the different designs of the approximation spaces considered are precisely compared in Section 5.1. The performance of the HNA BEM using collocation is finally demonstrated in Section 5.3 in which we show that the computational cost of the method is frequency independent. The conclusions of the present work and some opportunities for future work are finally exposed in Chapter 6.

Chapter 2

Boundary integral equation

2.1 Wave scattering problem

We describe here the two-dimensional wave scattering problem that we propose to solve in this work, as illustrated in Figure 2.1. We consider a time harmonic plane wave as incident field u^i with wave number $k \in \mathbb{R}$, $k > 0$ and direction given by the unit vector $\mathbf{d} = (d_1, d_2) \in \mathbb{R}^2$. We have

$$u^i(\mathbf{x}) = e^{ik\mathbf{x}\cdot\mathbf{d}}, \quad \text{for } \mathbf{x} = (x_1, x_2) \in \mathbb{R}^2. \quad (2.1)$$

The domain of propagation is considered homogeneous so that we assume that the wave number k is constant throughout the domain. Note that the restriction to the case of harmonic waves is done for simplicity of the analysis but more general time dependence can be straightforwardly obtained by combining harmonic waves of different frequencies using Fourier synthesis.

The scattering objects are sound soft screens, that we assume to be the union of a finite number $n_s \in \mathbb{N}$ of open and colinear intervals $\{\Gamma_i\}_{i=1}^{n_s}$ such that

$$\Gamma = \bigcup_{i=1}^{n_s} \Gamma_i, \quad \Gamma_i = (s_{2i-1}, s_{2i}) \times \{0\} \subset \mathbb{R}^2, \quad i = 1, \dots, n_s, \quad (2.2)$$

where $0 = s_1 < s_2 < \dots < s_{2n_s} = L \in \mathbb{R}$. The domain of propagation D of the waves is then

$$D = \mathbb{R}^2 \setminus \bar{\Gamma}, \quad (2.3)$$

where $\bar{\Gamma}$ is the closure of Γ .

Let $C^2(D)$ be the space of twice continuously differentiable functions on D . Let also $W_{\text{loc}}^1(D) := \{u \in L_{\text{loc}}^2(D) \mid \nabla u \in L_{\text{loc}}^2(D)\}$, where ∇u denotes the weak gradient

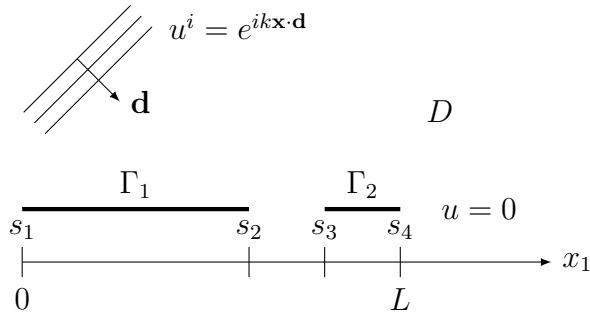


Figure 2.1: Sketch of the wave scattering problem for $n_s = 2$.

of u and $L_{\text{loc}}^2(D)$ is the set of locally integrable functions u on D . The total field $u \in C^2(D) \cap W_{\text{loc}}^1(D)$ is composed of the incident field u^i and the scattered field u^s so that $u = u^i + u^s$. The field u is found as the solution of the Helmholtz equation with Dirichlet boundary condition:

$$\begin{cases} \Delta u + k^2 u = 0, & \text{in } D, \\ u = 0, & \text{on } \Gamma. \end{cases} \quad (2.4a)$$

$$(2.4b)$$

The domain of propagation D is unbounded hence requiring an additional condition on the field reflected by the scattering obstacle at infinity. Explicitly, we assume that the scattered field u^s satisfies the Sommerfeld radiation condition at infinity,

$$\frac{\partial u^s}{\partial r} - iku^s = o(r^{-1/2}), \quad \text{uniformly as } r = |\mathbf{x}| \rightarrow \infty. \quad (2.5)$$

The wave scattering problem that we are going to study is given by the PDE (2.4a) and the two boundary conditions (2.4b) and (2.5).

We assume in the following that all lengths have been conveniently nondimensionalised with respect to a typical length scale so that the wave number k is nondimensional.

2.2 Boundary Integral Equation

We now give the reformulation of the problem as a boundary integral equation. The rigorous analysis of the scattering by two-dimensional planar screens is in the context of the fractional Sobolev spaces $H^{1/2}(\Gamma)$ and $\tilde{H}^{-1/2}(\Gamma)$, the precise definition of which are given, for instance, in [9, Section 2.] or [23].

We first recall the fundamental solution of the Helmholtz equation in two dimensions [8]

$$\Phi_k(\mathbf{x}, \mathbf{y}) = \frac{i}{4} H_0^{(1)}(k|\mathbf{x} - \mathbf{y}|), \quad \mathbf{x}, \mathbf{y} \in \mathbb{R}^2, \quad (2.6)$$

where $H_0^{(1)}$ is the Hankel function of the first kind or order zero.

We define the single layer potential $\mathcal{S}_k : \tilde{H}^{-1/2}(\Gamma) \rightarrow C^2(D) \cap W_{\text{loc}}^1(\mathbb{R}^2)$ which, for $\phi \in L^p(\Gamma)$ and $p > 1$, is represented by the integral formulation [8]

$$\mathcal{S}_k \phi(\mathbf{x}) = \int_{\Gamma} \Phi_k(\mathbf{x}, \mathbf{y}) \phi(\mathbf{y}) \, ds(\mathbf{y}), \quad \mathbf{x} \in D. \quad (2.7)$$

The single layer potential can be thought of in physical terms as an infinite distribution, on the boundary of the screen Γ , of elementary source terms $\Phi_k(\mathbf{x}, \cdot)$ with respective density ϕ . The representation formula holds [9, 16]

$$u(\mathbf{x}) = u^i(\mathbf{x}) - \mathcal{S}_k \left[\frac{\partial u}{\partial n} \right] (\mathbf{x}), \quad \mathbf{x} \in D, \quad (2.8)$$

where

$$\left[\frac{\partial u}{\partial n} \right] = \partial_{\mathbf{n}}^+(\chi u) - \partial_{\mathbf{n}}^-(\chi u) \quad (2.9)$$

and χ is an arbitrary element of

$$C_{0,1}^{\infty}(\mathbb{R}^2) := \{ \phi \in C_0^{\infty}(\mathbb{R}^2) \mid \phi = 1 \text{ in some neighbourhood of } \Gamma \}. \quad (2.10)$$

The normal derivative operators $\partial_{\mathbf{n}}^{\pm}$ are precisely defined in [9].

We define the single layer boundary integral operator $S_k : \tilde{H}^{-1/2}(\Gamma) \rightarrow H^{-1/2}(\Gamma)$ which, for $\phi \in L^p(\Gamma)$ and $p > 1$, is represented by the integral formulation [8]

$$S_k \phi(\mathbf{x}) = \int_{\Gamma} \Phi_k(\mathbf{x}, \mathbf{y}) \phi(\mathbf{y}) \, ds(\mathbf{y}), \quad \mathbf{x} \in \Gamma. \quad (2.11)$$

From (2.8), taking traces onto the boundary Γ and applying the jump relations connecting \mathcal{S}_k and S_k , the wave scattering problem can be reformulated as [8]:

Find $\left[\frac{\partial u}{\partial n} \right] \in \tilde{H}^{-1/2}(\Gamma)$ such that

$$\int_{\Gamma} \Phi_k(\mathbf{x}, \mathbf{y}) \left[\frac{\partial u}{\partial n} \right] (\mathbf{y}) \, ds(\mathbf{y}) = u^i \Big|_{\Gamma} (\mathbf{x}), \quad \mathbf{x} \in \Gamma. \quad (2.12)$$

Equation (2.12) is the boundary integral equation of the first kind that we propose to solve. There exists no simple closed form solution to this BIE and one needs to solve it numerically, as we detail below.

An important question is the well-posedness of the problem given by (2.12). Wavenumber-explicit coercivity and continuity estimates for S_k have been recently derived [9, 16]. These results ensure existence and uniqueness of the solution to the BIE via application of the Lax-Milgram lemma.

We also mention that other formulations are possible. In particular, it is possible to obtain BIE of the second kind, which could be better conditioned, see for instance [6].

2.3 High-Frequency Asymptotics

The boundary integral equation (2.12) can be solved numerically using a conventional boundary element method. This involves picking a finite dimensional subspace of $\tilde{H}^{-1/2}(\Gamma)$ in which to look for a solution and solve the integral equation in variational form using a Galerkin method, or via collocation, by enforcing the integral equation to hold exactly at finite number set of points. Even though these methods are controllably accurate, they would be numerically tractable only for low or moderate frequencies. Indeed, to correctly capture the oscillations of the solution, the number of degrees of freedom should scale at least linearly with the wave number k [8]. The method would then become prohibitively expensive when k is large. It is true that other approaches can be considered in the high frequency regime, and a number of asymptotic theories such as the Geometrical Theory of Diffraction are available. However such theories are arbitrarily accurate only in the limit as k tends to infinity. As a result, there is large gap of frequencies for which no computationally feasible method can provide an accurate solution. To overcome this difficulty, the key idea that has been proposed [8] is to enrich the approximation space (defined precisely in Chapter 3) with the known asymptotic behaviour of the solution given by asymptotic theories.

We now introduce the high-frequency asymptotics that we rely on to build our hybrid numerical-asymptotic approximation space. We represent a point \mathbf{x} on the boundary Γ using the following parametrisation involving the arc length s

$$\mathbf{x}(s) = (s, 0), \quad \text{where} \quad s \in \tilde{\Gamma} := \bigcup_{i=1}^{n_s} (s_{2i-1}, s_{2i}). \quad (2.13)$$

On each screen (s_{2i-1}, s_{2i}) , the Geometrical Theory of Diffraction gives an approximation of the jump $\left[\frac{\partial u}{\partial n}\right]$ in the high frequency regime of the form

$$\left[\frac{\partial u}{\partial n}\right](\mathbf{x}(s)) \approx 2\frac{\partial u^i}{\partial n}(\mathbf{x}(s)) + Ae^{iks} + Be^{-iks}, \quad \text{as } k \rightarrow +\infty, \quad (2.14)$$

where A and B are the diffraction coefficients which are expected to be slowly varying on the scatterer [5]. The first term is the geometrical optic approximation and represents the sum of the incident and reflected waves on the obstacle. It is the leading term in the asymptotic behaviour and, used alone in (2.8), corresponds to the 'physical optic' or 'Kirchoff' approximation. The two other terms represent the diffracted waves emerging from the ends of each screen.

The construction of the hybrid numerical-asymptotic approximation space is supported by a regularity result from [16, Theorem 4.1], that we restate in Theorem 2.1. Standard elliptic regularity results ensure continuity in D of the solution u of the wave scattering problem described in Section 2.1. Since, in addition, $u(\mathbf{x}) \sim u^i(\mathbf{x})$ as $\mathbf{x} \rightarrow \infty$, $\mathbf{x} \in D$, we have that

$$M(u) := \sup_{\mathbf{x} \in D} |u(\mathbf{x})| \quad (2.15)$$

exists and is finite [16]. We define also

$$l_{\min} := \min_{i=1, \dots, n_s} (s_{2i-1} - s_{2i}). \quad (2.16)$$

We now quote the regularity result.

Theorem 2.1. *Let $kl_{\min} \geq c_0$ for some $c_0 > 0$. For $i = 1, \dots, n_s$, we have*

$$\left[\frac{\partial u}{\partial n} \right] (\mathbf{x}(s)) = 2 \frac{\partial u^i}{\partial n} (\mathbf{x}(s)) + \nu_i^+(s - s_{2i-1}) e^{iks} + \nu_i^-(s_{2i} - s) e^{-iks}, \quad s \in (s_{2i-1}, s_{2i}). \quad (2.17)$$

The functions ν_i^\pm are analytic in the right half-plane and non-oscillatory. Explicitly, there exists $C_1 \in \mathbb{R}$, $C_1 > 0$, which depends only on c_0 , such that in the right-hand side plane $\Re(s) > 0$, we have

$$|\nu_i^\pm(s)| \leq C_1 M(u) k |ks|^{-1/2}, \quad \Re(s) > 0. \quad (2.18)$$

For a proof of this result, we refer to [17].

Note that the bound (2.18) is sharp in that the functions $s \mapsto \nu_i^\pm(s)$ are actually equivalent to the bound as $s \rightarrow 0$. Hence $\nu_i^\pm \notin L^2(\Gamma)$. Following Remark 4.2 in [16], we note also that the Cauchy integral formula for derivatives yields bounds of the form

$$|\nu_i^{\pm(n)}(s)| \leq c_n C_1 M(u) k^{1/2} s^{-(n+1/2)}, \quad s > 0, \quad n \in \mathbb{N}, \quad n \geq 1, \quad (2.19)$$

for each derivatives $\nu_i^{\pm(n)}$ and where the constants $c_n \in \mathbb{R}$, $c_n > 0$ only depend on n . The fact that these bounds (2.19) have the same k -dependence for all n implies that the functions ν_i^\pm are non-oscillatory. Finally note that they encapsulate all the contributions from the multiple-diffracted waves along the boundary.

Using the representation (2.17) for the unknown $\left[\frac{\partial u}{\partial n} \right]$ leaves only the amplitude functions ν_i^\pm to compute numerically. Let

$$\phi = \left[\frac{\partial u}{\partial n} \right], \quad \text{and} \quad \Psi = 2 \frac{\partial u^i}{\partial n}. \quad (2.20)$$

In addition, we denote by φ the difference between ϕ and its geometrical optic approximation Ψ scaled by $1/k$, such that

$$\varphi(s) = \frac{1}{k}(\phi(\mathbf{x}(s)) - \Psi(\mathbf{x}(s))), \quad s \in \tilde{\Gamma}. \quad (2.21)$$

The wave scattering problem can now be reformulated as:

Find φ such that

$$S_k \varphi = \frac{1}{k} \left(u^i \Big|_{\Gamma} - 2S_k \frac{\partial u^i}{\partial n} \right). \quad (2.22)$$

The explicit integral form of (2.22) reads

$$\int_{\Gamma} \Phi_k(\mathbf{x}, \mathbf{y}) \varphi(\mathbf{y}) \, ds(\mathbf{y}) = \frac{1}{k} \left(u^i \Big|_{\Gamma}(\mathbf{x}) - 2 \int_{\Gamma} \Phi_k(\mathbf{x}, \mathbf{y}) \frac{\partial u^i}{\partial n}(\mathbf{y}) \, ds(\mathbf{y}) \right), \quad \mathbf{x} \in \Gamma. \quad (2.23)$$

We propose to solve (2.22) using a boundary element method with an approximation space (defined precisely in the next section) based on the decomposition, inspired by Theorem 2.1,

$$\varphi(s) = \frac{1}{k} (\nu_i^+(s - s_{2i-1})e^{iks} + \nu_i^-(s_{2i} - s)e^{-iks}), \quad s \in (s_{2i-1}, s_{2i}). \quad (2.24)$$

Chapter 3

Numerical method

3.1 Hybrid Numerical-Asymptotic approximation space

The numerical method we now present is based on a hybrid numerical-asymptotic approximation space using the result given in Theorem 2.1. The unknown φ , solution to the BIE (2.22), takes the form of (2.24) in which the functions ν_i^\pm are approximated by piecewise polynomials on each screen. Note that it is not the unknown φ itself which is approximated numerically as in more standard numerical methods but rather only the diffraction amplitudes ν_i^\pm .

We now describe the meshes we use and on which we rely to define precisely the piecewise polynomial functions of the approximation space. We consider two different approximation strategies on each screen Γ_i for $i = 1, \dots, n_s$, both involving geometrical grading towards the singularities:

1. Overlapping meshes, used for instance in [16] or [2]: this strategy consists in constructing two independent meshes for the two components $\nu_i^\pm e^{\pm iks}$ of the unknown, the right (+) and left (−) propagating waves. From the geometrical theory of diffraction [5], we know that the two amplitude functions ν_i^\pm do not have the same behaviour on the screen Γ_i . The right propagating wave component $\nu_i^+(s)e^{+iks}$ has a (square-root) singularity on the left of the screen $s = s_{2i-1}$, and is graded accordingly. For the left propagating wave $\nu_i^-(s)e^{-iks}$, the singularity is present at the right of the screen $s = s_{2i}$, where a similar grading is applied. A sketch of two overlapping meshes corresponding to this description is given in Figure 3.1a for a single screen.

2. Single mesh: the alternative strategy involves only one mesh on which both components $\nu_i^\pm(s)e^{\pm iks}$ are evaluated. The mesh must therefore be graded at both ends. A similar meshing strategy, using a single mesh but with a different type of grading, is described for instance in [12] for a related problem. As a practical note, this type of mesh can be computed as the intersection of the two overlapping meshes. See Figure 3.1b for a sketch of a single-mesh configuration.

The overlapping-type meshing strategy is tailored exactly to be able to capture the two unknown terms in the unknown φ , in particular their own singularities. An associated difficulty, from an implementation point of view, is the necessity to keep track of the elements in the two meshes. In our two-dimensional problem with planar screens, this complication remains limited, but can however be an issue in the perspective of tackling problems in three dimensions. This remark is valid for both Galerkin or collocation methods. In the latter context, there is an additional complexity coming from the distribution of the collocation on the two meshes, as allocating two points almost at the same position but on the two different meshes leads immediately to bad conditioning of the matrix (singular matrix if the position is exactly the same), see Section 3.3 and also [2] for more details.

The single mesh strategy do not suffer from these issues. In particular, the allocation of the collocation points is easier. The strategy is however not exempt of conditioning problems. The fact to have both the two oscillatory components of the unknown in each element makes it difficult to numerically separate their two contributions on the small (with respect to the wavelength $\lambda = 2\pi/k$) elements near the corners of the screens, as the oscillatory factors $e^{\pm iks}$ will almost match. This leads also to ill-conditioning; see [2] and the end of the current section for more details and a way of dealing with this issue. The main drawback of the single-type meshing comes from the fact introduction of unnecessary degrees of freedom in the approximation space. The amplitude function ν_i^+ is indeed approximated by far more basis functions near the right corner of the screen $s = s_{2i}$ than necessary, and similarly for the function ν_i^- near the left corner $s = s_{2i-1}$.

We now give some more details on the practical construction of the meshes, starting with the overlapping configuration. Consider the screens $\Gamma = \bigcup_{i=1}^{n_s} \Gamma_i$ described in (2.2). For each $i = 1, \dots, n_s$, let $(n_i^+, n_i^-) \in \mathbb{N}^2$, such that $n_i^+ \geq 1$ and $n_i^- \geq 1$. The mesh on the screen Γ_i and supporting the right propagating wave $\nu_i^+ e^{+iks}$ is denoted $\mathcal{M}_{n_i^+}^+(\Gamma_i)$ where n_i^+ is the number of layers or elements in the mesh. It is given by

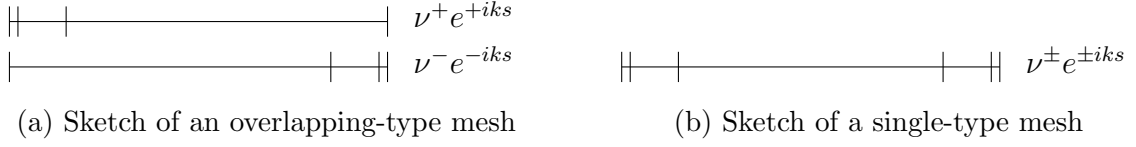


Figure 3.1: Illustrations of the two mesh configurations considered on a single screen. Grading parameter $\sigma = 0.15$.

the set of points $\{x_j^+\}_{j=0}^{n_i^+}$ such that:

$$x_0^+ := s_{2i-1}, \quad x_j^+ := s_{2i-1} + \sigma^{n_i^+ - j}(s_{2i} - s_{2i-1}), \quad j = 1, \dots, n_i^+. \quad (3.1)$$

In [28], the theoretical optimum value for the grading parameter σ in such geometric meshes is given to be $\sigma = (\sqrt{2} - 1)^2 \approx 0.17$. Practical experience suggests that a slightly more severe grading is desirable and in [16] the choice $\sigma = 0.15$ is recommended. This is the value taken in all the numerical experiments presented in this work. The mesh $\mathcal{M}_{n_i^-}^{\circ-}(\Gamma_i)$ supporting the left propagating wave $\nu_i^- e^{-iks}$ on the same screen Γ_i and using n_i^- layers contains the points $\{x_j^-\}_{j=0}^{n_i^-}$ such that:

$$x_j^- := s_{2i} - \sigma^j(s_{2i} - s_{2i-1}), \quad j = 0, \dots, n_i^- - 1, \quad x_{n_i^-}^- = s_{2i}. \quad (3.2)$$

The single-type mesh $\mathcal{M}_{n_i^+, n_i^-}^s(\Gamma_i)$ is obtained from the two previous sets of points by intersection

$$\mathcal{M}_{n_i^+, n_i^-}^s(\Gamma_i) := \mathcal{M}_{n_i^+}^{\circ+}(\Gamma_i) \cap \mathcal{M}_{n_i^-}^{\circ-}(\Gamma_i). \quad (3.3)$$

Let $a, b \in \mathbb{R}$, $a < b$ and $p \in \mathbb{N}$; we denote by $\mathcal{Q}_p(a, b)$ the space of continuous polynomials on the interval (a, b) of degree at most p

$$\mathcal{Q}_p(a, b) := \left\{ \rho : [a, b] \rightarrow \mathbb{C} \mid \deg(\rho) \leq p \right\}. \quad (3.4)$$

Let $n \in \mathbb{N}$, $n \geq 1$ and $c, d \in \mathbb{R}$, $c < d$. We consider a general mesh $\mathcal{M}_n = \{x_i\}_{i=0}^n$ with n elements, on the interval $[c, d]$. Let $\mathbf{p} \in \mathbb{N}^n$; following [16] we define $\mathcal{P}_{\mathbf{p}}(\mathcal{M}_n)$ the space of piecewise polynomials with degrees given by \mathbf{p} on the mesh \mathcal{M}_n as

$$\mathcal{P}_{\mathbf{p}}(\mathcal{M}_n) := \left\{ \rho : [c, d] \rightarrow \mathbb{C} \mid \rho|_{(x_i, x_{i+1})} \in \mathcal{Q}_{\mathbf{p}_i}(x_i, x_{i+1}), \quad i = 0, \dots, n-1 \right\}. \quad (3.5)$$

For each $i = 1, \dots, n_s$, we denote respectively by N_i^+ and N_i^- the total number of basis functions with support included in Γ_i for approximating the right ν_i^+ and left ν_i^- components. Explicitly we have $N_i^+ = n_i^+$ and $N_i^- = n_i^-$ if an overlapping-mesh configuration is considered and we have $N_i^+ = N_i^- = n_i^+ + n_i^- - 1$ if a single-mesh configuration is considered. In the latter case, the definition assumes that no

interior points coincide in the two sets intersected in (3.3), but trivial adaptation can be carried out if this is not the case. For each $i = 1, \dots, n_s$, choose $(\mathbf{p}_i^+, \mathbf{p}_i^-) \in \mathbb{N}^{N_i^+} \times \mathbb{N}^{N_i^-}$. The simplest choice for the vector of degrees \mathbf{p}_i^\pm would be to take all degrees constant, $\mathbf{p}_i^\pm = p$, $i = 1, \dots, N_i^\pm$. However, for reasons of efficiency and stability, it is standard practice to decrease the degree of the polynomials linearly towards the singularity [16]. For the overlapping meshing strategy we take

$$\mathbf{p}_i^\pm = \begin{cases} p - \lfloor \frac{\alpha(N_i^\pm + 1 - i)}{N_i^\pm} p \rfloor, & 1 \leq i \leq N_i^\pm - 1, \\ p, & i = N_i^\pm, \end{cases} \quad (3.6)$$

where α is chosen in $[0, 1]$. For the single-mesh strategy we take

$$\mathbf{p}_i^+ = \begin{cases} p - \lfloor \frac{\alpha(N_i^+ + 1 - i)}{N_i^+} p \rfloor, & 1 \leq i \leq N_i^+ - 1, \\ p, & i = n_i^+, \\ p - \lfloor \frac{\alpha i}{N_i^-} p \rfloor, & 1 \leq i \leq N_i^- - 1, \end{cases} \quad (3.7a)$$

and

$$\mathbf{p}_i^- = \begin{cases} p - \lfloor \frac{\alpha(N_i^- + 1 - i)}{N_i^-} p \rfloor, & 1 \leq i \leq N_i^- - 1, \\ p, & i = n_i^-, \\ p - \lfloor \frac{\alpha i}{N_i^+} p \rfloor, & 1 \leq i \leq N_i^+ - 1, \end{cases} \quad (3.7b)$$

where α is chosen similarly. For $\alpha = 0$ we recover the case of constant degrees for all polynomials and for $\alpha = 1$ we have the most reduction of the degree of the polynomials towards the singularity. The latter choice gives better conditioning [16] and importantly reduces the number of degrees of freedom required. This choice of parameter $\alpha = 1$ is confirmed by our numerical experiments for the two meshing strategies; see Section 5.1 for more details.

We are now able to give a proper definition of our hybrid numerical-asymptotic (HNA) approximation space, noted \mathcal{S}_N , where N denotes the total number of degrees of freedom of the numerical scheme (calculated later). We define the spaces S_i^+ and S_i^- such that

$$S_i^+ := \left\{ s \mapsto \rho(s) e^{+iks} \mid \rho \in \mathcal{P}_{\mathbf{p}_i^+}(\mathcal{M}^+(\Gamma_i)) \right\}, \quad (3.8a)$$

$$S_i^- := \left\{ s \mapsto \rho(s) e^{-iks} \mid \rho \in \mathcal{P}_{\mathbf{p}_i^-}(\mathcal{M}^-(\Gamma_i)) \right\}, \quad (3.8b)$$

where

$$\mathcal{M}^+(\Gamma_i) := \mathcal{M}_{n_i^+}^{o^+}(\Gamma_i), \quad \mathcal{M}^-(\Gamma_i) := \mathcal{M}_{n_i^-}^{o^-}(\Gamma_i), \quad (3.9)$$

for an overlapping-mesh configuration, and

$$\mathcal{M}^+(\Gamma_i) := \mathcal{M}_{n_i^+, n_i^-}^s(\Gamma_i), \quad \mathcal{M}^-(\Gamma_i) := \mathcal{M}_{n_i^+, n_i^-}^s(\Gamma_i), \quad (3.10)$$

for a single-mesh configuration. The approximation space \mathcal{S}_N then reads

$$\mathcal{S}_N := \text{span} \left\{ \bigcup_{i=1}^{n_s} (S_i^+ \cup S_i^-) \right\}. \quad (3.11)$$

Note that elements of \mathcal{S}_N are of the form of (2.24) and are, by the result in Theorem 2.1 well-suited to approximate the exact solution φ . The total number of degrees of freedom in the numerical scheme N is given by

$$N := \dim(\mathcal{S}_N) = \sum_{i=1}^{n_s} \left(\sum_{j=1}^{N_i^+} ((\mathbf{p}_i^+)_j + 1) + \sum_{j=1}^{N_i^-} ((\mathbf{p}_i^-)_j + 1) \right). \quad (3.12)$$

For the single-type mesh, an issue we already mentioned and highlighted in [2] comes from the relatively short elements with length $l \ll \lambda$ at both ends. These elements are supposed to support both the left e^{-iks} and right e^{+iks} propagating waves that almost match in this case and leads to ill-conditioning. One can cope with this quite easily by setting to zero the coefficient of the wave which is not singular at the end under consideration. This amounts to modifying the approximation space \mathcal{S}_N as follows. For each screen Γ_i with $i = 0, \dots, n_s$, let

$$\left\{ \begin{array}{l} \tilde{\mathcal{M}}_{n_i^+}^{o+}(\Gamma_i) := \{x_0^+\} \cup \left\{ x_i^+ \in \mathcal{M}_{n_i^+}^{o+}(\Gamma_i) \mid x_i^+ - x_{i-1}^+ \geq \beta \frac{2\pi}{k}, i = 1, \dots, n_i^+ \right\}, \\ \tilde{\mathcal{M}}_{n_i^-}^{o-}(\Gamma_i) := \{x_0^-\} \cup \left\{ x_i^- \in \mathcal{M}_{n_i^-}^{o-}(\Gamma_i) \mid x_i^- - x_{i-1}^- \geq \beta \frac{2\pi}{k}, i = 1, \dots, n_i^- \right\}, \end{array} \right. \quad (3.13)$$

where β is an arbitrary parameter. Numerical experiments suggests that β should be $\mathcal{O}(1)$. In practical computations we take $\beta = 2$. Note that we implicitly incorporate some k -dependency in the approximation space as we measure the shortness of the elements with respect to the wavelength λ of the problem. For a fixed initial number of layers n_i^\pm , the number of degrees of freedom that are used increases with the wave number k , even though it is bounded uniformly in k . We then redefine the meshes $\mathcal{M}^+(\Gamma_i)$ and $\mathcal{M}^-(\Gamma_i)$ in (3.10) as

$$\mathcal{M}^+(\Gamma_i) := \mathcal{M}_{n_i^+}^{o+}(\Gamma_i) \cap \tilde{\mathcal{M}}_{n_i^-}^{o-}(\Gamma_i), \quad \mathcal{M}^-(\Gamma_i) := \tilde{\mathcal{M}}_{n_i^+}^{o+}(\Gamma_i) \cap \mathcal{M}_{n_i^-}^{o-}(\Gamma_i). \quad (3.14)$$

The definitions of the spaces S_i^+ and S_i^- in (3.8), the approximation space \mathcal{S}_N in (3.11) and the number of degrees of freedom N in (3.12) are left unchanged. Numerical experimentations have confirmed the efficiency of this modification. In addition, we note that the refinement for both basis functions at both ends of each screens in the case of the single-type meshing strategy results in an unnecessary increased number

of degrees of freedom. In this respect, dropping one basis function when the elements are too short helps to minimise this effect.

We now quote the best approximation result given in [16, Theorem 5.1], that ensures exponential convergence of a member of \mathcal{S}_N towards the unknown φ as the maximum degree of the polynomials p increases. It relies on the regularity result given in Theorem 2.1 and is proven in [16] for the approximation space based on the overlapping meshes. A similar result is believed to hold for the similar approximation space using a single mesh.

Theorem 3.1. *Let $kl_{\min} \geq c_0 > 0$. Suppose that $N_i^\pm = N_e$ and $\mathbf{p}_i^\pm = \mathbf{p}$ for each $i = 1, \dots, n_s$, where \mathbf{p} is defined according to (3.6) and N_e is such that $N_e \geq cp$ for some constant $c \in \mathbb{R}$, $c > 0$. Choose any $0 < \epsilon < 1/2$. Then there exists a constant $C_2 \in \mathbb{R}$, $C_2 > 0$, depending only on ϵ , σ , n_s and c_0 ; and a constant $\tau \in \mathbb{R}$, $\tau > 0$, depending only on ϵ , σ , α and c such that*

$$\inf_{v \in \mathcal{S}_N} \|\varphi - v\|_{\tilde{H}_k^{-1/2}(\Gamma)} \leq C_2 M(u) k^{-1} (kL)^\epsilon e^{-p\tau}. \quad (3.15)$$

For a proof of this result we refer to [16].

3.2 Collocation method

A possible choice for solving the BIE (2.12) is to use a Galerkin framework after reformulating (2.12) in variational form. This approach has been used successfully for the overlapping mesh case in [16]. However, the method requires numerical evaluation of oscillatory double integrals for two-dimensional problems. When three-dimensional problems are considered, the implementation of the Galerkin method appears to be even more challenging. The collocation method could be in this respect a simpler method to implement, in particular for generalisation to higher dimensions. A main advantage over the Galerkin method is that, for two-dimensional problems, the oscillatory integrals that one needs to evaluate are only single integrals. However the theoretical analysis of the convergence of collocation methods for the scalar Helmholtz equation is less available [30, page 318], compared to analysis for the Galerkin method. For instance, a full convergence analysis of a Galerkin HNA BEM method has been presented in [16], with frequency-explicit error estimates, for the scattering problem under consideration. The main purpose of this work is then to determine whether a collocation method is appropriate and efficient to solve such problems. In particular,

the question of the robustness of the method with respect to the position of the collocation points on the boundary is an important question. A related question is the evolution of the conditioning of the numerical problem with respect to the number of degrees of freedom. We shall address all these points in the following.

Choose, for the wave scattering problem described in Section 2.1, a HNA approximation space \mathcal{S}_N with N degrees of freedom, as defined in Section 3.1. Choose independently a set of N distinct collocation points $\mathcal{C}_N = \{c_n\}_{n=1}^N$ distributed on the screens $\Gamma = \bigcup_{i=1}^{n_s} \Gamma_i$. This choice selects a numerical approximation $\varphi_N \in \mathcal{S}_N$ of the solution φ of the BIE (2.22) and is computed precisely as follows. Let us introduce the following notation for $\varphi_N : \tilde{\Gamma} \rightarrow \mathbb{C}$

$$\varphi_N := s \mapsto \sum_{i=1}^{n_s} \left[\sum_{j=1}^{N_i^+} \sum_{m=0}^{(\mathbf{p}_i^+)_j} \left(\nu_{i,j,m}^+ \rho_{i,j,m}^+(s) e^{+iks} \right) + \sum_{j=1}^{N_i^-} \sum_{m=0}^{(\mathbf{p}_i^-)_j} \left(\nu_{i,j,m}^- \rho_{i,j,m}^-(s) e^{-iks} \right) \right], \quad (3.16)$$

where $\{\nu_{i,j,m}^\pm \in \mathbb{C}\}_{i,j,m}$ are the N degrees of freedom and $\{\rho_{i,j,m}^\pm\}_{i,j,m}$ are polynomials that we define now. No special property is required for the polynomials used. Note that this is not true for Galerkin methods, for which particular choices of polynomials are sometimes preferable over others, depending on their properties. For instance, orthogonality can increase matrix sparsity of the linear system for a Galerkin method. The most simple choice for our collocation method has therefore been made, namely we use monomials such that

$$\hat{\rho}_p := [-1, 1] \rightarrow \mathbb{R}, \quad \text{with} \quad \hat{\rho}_p(s) := \lambda_p s^p, \quad p \in \mathbb{N}. \quad (3.17)$$

The factors $\{\lambda_p \in \mathbb{R}\}_{p \in \mathbb{N}}$ are normalisation constants. In our numerical experiments the simple choice $\lambda_p = 1$ for $p \in \mathbb{N}$ has been made. However, a particular normalisation of these polynomials might help with the conditioning of the matrix. The basis of polynomials $\{\hat{\rho}_p\}_{p \in \mathbb{N}}$ are defined on $[-1, 1]$. They are translated and scaled to be supported on the subintervals of the meshes as necessary. For each screen Γ_i with $i = 0, \dots, n_s$, the meshes (3.9) and (3.14) are denoted as $\mathcal{M}^+(\Gamma_i) = \{x_j^+\}_{j=0}^{N_i^+}$ and $\mathcal{M}^-(\Gamma_i) = \{x_j^-\}_{j=0}^{N_i^-}$. We have

$$\rho_{i,j,m}^+(s) := \begin{cases} \hat{\rho}_m \left(\frac{2}{x_{j+1}^+ - x_j^+} \left(s - \frac{x_j^+ + x_{j+1}^+}{2} \right) \right), & s \in (x_j^+, x_{j+1}^+), \\ 0, & s \in \tilde{\Gamma} \setminus (x_j^+, x_{j+1}^+), \end{cases} \quad m = 0, \dots, (\mathbf{p}_i^+)_j, \quad (3.18a)$$

$$\rho_{i,j,m}^-(s) := \begin{cases} \hat{\rho}_m \left(\frac{2}{x_{j+1}^- - x_j^-} \left(s - \frac{x_j^- + x_{j+1}^-}{2} \right) \right), & s \in (x_j^-, x_{j+1}^-), \\ 0, & s \in \tilde{\Gamma} \setminus (x_j^-, x_{j+1}^-), \end{cases} \quad m = 0, \dots, (\mathbf{p}_i^-)_j. \quad (3.18b)$$

Our approximate solution φ_N in (3.16) is completely described now except for the set of degrees of freedom $\{\nu_{i,j,m}^\pm \in \mathbb{C}\}_{i,j,m}$. At each collocation point $c_n \in \mathcal{C}_N$, for $n = 1, \dots, N$, we require

$$\sum_{i=1}^{n_s} \int_{\Gamma_i} \varphi_N|_{\Gamma_i}(s) \Phi_k(c_n, s) \, ds, = u^i|_{\Gamma}(c_n) - \sum_{i=1}^{n_s} \int_{\Gamma_i} 2 \frac{\partial u^i}{\partial n}(s) \Phi_k(c_n, s) \, ds. \quad (3.19)$$

Choose an ordering for the set of degrees of freedom $\{\nu_{i,j,m}^\pm \in \mathbb{C}\}_{i,j,m}$ and collect them in the vector $\boldsymbol{\nu} \in \mathbb{C}^N$. For each collocation point $c_n \in \mathcal{C}_N$, with $n = 1, \dots, N$, also collect, using the same ordering, the set

$$\left\{ \int_{\Gamma_i} \rho_{i,j,m}^\pm(s) \Phi_k(c, s) e^{\pm iks} \, ds \right\}_{i,j,m} \quad (3.20)$$

into the n^{th} line \mathbf{M}_n of the matrix $\mathbf{M} \in \mathbb{C}^{N \times N}$. For each collocation point $c_n \in \mathcal{C}_N$, with $n = 1, \dots, N$, let finally the n^{th} component \mathbf{F}_n of the vector $\mathbf{f} \in \mathbb{C}^N$ be

$$\mathbf{f}_n := u^i|_{\Gamma}(c_n) - \sum_{i=1}^{n_s} \int_{\Gamma_i} 2 \frac{\partial u^i}{\partial n}(s) \Phi_k(c_n, s) \, ds. \quad (3.21)$$

These definitions allow to recast the system of equations (3.19) in the form of the linear system

$$\mathbf{M} \boldsymbol{\nu} = \mathbf{f}. \quad (3.22)$$

The matrix \mathbf{M} is dense but its size, $N \times N$, is moderate as N is typically at most a few hundreds. The linear system is then solved using standard direct solvers and the numerical solution φ_N is completely determined from $\boldsymbol{\nu} = \mathbf{M}^{-1}\mathbf{f}$.

3.3 Allocation of the collocation points

One question we have not answered yet is the allocation of the collocation points $\mathcal{C}_N = \{c_n\}_{n=1}^N$ distributed on the screens Γ . This is not an easy question and different approaches can be considered.

Given our approximation space \mathcal{S}_N , the simplest choice is to distribute $p+1$ points in an element of the mesh supporting a polynomial of degree p . By doing this, we allocate the N points available.

The local allocation of the collocation points on each mesh element can then be done in different ways and two of them were investigated. One naive choice is to distribute them uniformly. Suppose that we need to allocate N_c collocation points on

a segment $[a, b]$, which can be a whole screen or only an element of it. We place the points $\{c_i\}_{i=1}^{N_c}$ according to

$$c_i = a + \left(i - \frac{1}{2}\right) \frac{b - a}{N_c}, \quad i = 1, \dots, N_c. \quad (3.23)$$

Note that it is not possible to place collocation points at the ends of the screens where singularities in the solution occur.

However, given the analogy of a collocation method with a projection operator defined by interpolation [22, Section 13.3], one may consider other types of distributions. In particular, to avoid possible Runge phenomena, Chebyshev grids can be considered. Since it is not possible to place collocation points at the ends of the screens, the roots of the Chebyshev polynomials of the first kind, the so-called Chebyshev nodes, are used. The N_c points $\{c_i\}_{i=1}^{N_c}$ on the segment $[a, b]$ are then placed according to [31]

$$c_i = \frac{1}{2}(a + b) + \frac{1}{2}(b - a) \cos\left(\frac{2i - 1}{N_c}\pi\right), \quad i = 1, \dots, N_c. \quad (3.24)$$

These two allocation strategies are referred to as *local* strategies. An alternative choice is a *global* strategy for which the points are positioned on the screen independently of the mesh-elements. This latter approach might seem appropriate given the global nature of the BIO in (2.22). However, the results obtained from our implementation of the method using the global approach were unsatisfactory, and spurious oscillations in the numerical solution on the boundary were observed. We therefore only consider local distributions of the collocation points in the following.

We finish this section by a note on the conditioning of the matrix of the problem, related to the allocation of the collocation points in the overlapping meshing strategy. The main issue when using overlapping meshes, as we already pointed out in section 3.1, is that allocation of collocation points on each mesh may result in two points being relatively close to each other, which leads to ill-conditioning [2]. This is illustrated by the evolution of the condition number of the matrix \mathbf{M} with respect to the number of degrees of freedom, given in Section 5.1. A solution to this issue is to reposition the points by introducing some additional space between the two points. One then needs to built an heuristic strategy to reposition the points. No attempt in this direction has been made in this work.

Chapter 4

Numerical quadrature

4.1 Integral evaluation required by the method

The hybrid numerical-asymptotic collocation method described above requires, for the construction of the matrix \mathbf{M} in the linear system (3.22) and evaluation of the representation formula (2.8), the computation of integrals of the type

$$I_k = \int_a^b f(s) H_0^{(1)}(k|\mathbf{x} - s|) e^{i\theta ks} ds, \quad (4.1)$$

where $s \mapsto f(s)$ is a polynomial, $H_0^{(1)}$ is the Hankel function of the first kind of order zero, $(a, b) \subset \mathbb{R}$, $\mathbf{x} \in \mathbb{R}^2$ and θ , $k \in \mathbb{R}$ with $\theta \in \{\pm 1, d_1\}$ and $k > 0$. We review now the features that make integrals of this form difficult to evaluate using numerical quadrature.

In general $\mathbf{x} \in \mathbb{R}^2$, but let us first consider the particular case where \mathbf{x} is on the boundary Γ , so that $\mathbf{x} = x \in \mathbb{R}$. All the integrals involved in the computation of the linear system (3.22) are of this type. The Hankel function $H_0^{(1)}$ has a log-singularity at the origin [26, Section 10.7(i)], $H_0^{(1)}(x) \sim \frac{2i}{\pi} \ln(x)$, for $x \in \mathbb{R}$, $x > 0$. Hence if $x \in (a, b)$, this integral (4.1) is itself singular. If on the other hand $x \notin (a, b)$ but x is close to a or b , in a sense to be specified, then the integral is 'nearly singular' and still requires careful numerical treatment.

Furthermore, when the wave number k is large, the integral (4.1) is, in general, (but not always as we shall see) highly oscillatory. Define the exponentially scaled Hankel function $\tilde{H}_0^{(1)}(x) = H_0^{(1)}(x) e^{-ix}$, for $x \in \mathbb{R}$. Note that the e^{-ix} factor cancels the oscillations of the Hankel function for $x > 0$, so that $\tilde{H}_0^{(1)}$ is non-oscillatory for large $x > 0$ [26, Section 10.17(i)]. The integral (4.1) can then be rewritten as

$$I_k = \int_a^b f(s) \tilde{H}_0^{(1)}(k|x - s|) e^{ik(\theta s + |x - s|)} ds. \quad (4.2)$$

Hence, the oscillations are cancelled if $x < s$ and $\theta = -1$ or if $x > s$ and $\theta = 1$. If these conditions are not met however, the integral (4.1) becomes highly oscillatory as the wave number k increases, the oscillations being in this case only contained in the factor $e^{ik(\theta s + |x-s|)}$. Note that in the oscillatory case the phase of the oscillations, $k(\theta s + |x-s|)$, is linear in s . Standard integration routines such as Gaussian quadrature cannot evaluate highly oscillatory integrals efficiently and one must use specialised oscillatory quadrature techniques that we will present in Section 4.3.

Consider now that $\mathbf{x} = (x_1, x_2)$ in the integral (4.1) is in the domain $\mathbf{x} \in D$. We are confronted by integrals of this type if we wish to evaluate the solution in the domain via the representation formula (2.8). The integral (4.1) can no longer be singular but could still be difficult to evaluate when \mathbf{x} is close to the boundary Γ . The integral (4.1) is still oscillatory, and we can write

$$I_k = \int_a^b f(s) \tilde{H}_0^{(1)}(k|\mathbf{x} - s|) e^{ik(\theta s + \sqrt{(x_1-s)^2 + x_2^2})} ds. \quad (4.3)$$

The non-linearity of the phase of the oscillator makes the evaluation of such integrals more difficult in general than for the integral (4.2). wave field u in the domain of propagation D . No frequency independent quadrature rule has been implemented for this work, and we resorted to using standard quadrature rules when required. We refer to [21] and the references therein for some details on the oscillatory numerical quadrature methods available to evaluate integrals of the form of (4.3).

We shall now describe how the integrals of the form of (4.2) can be computed accurately with a computational cost which is independent of the wave number k .

4.2 Gauss-Legendre quadrature

The standard Gauss-Legendre quadrature rule is appropriate for integrals that are neither singular nor oscillatory. It belongs to the general class of Gauss quadrature methods approximating integrals by a weighted sum of function evaluations of the form [31]

$$\int_a^b \omega(s) f(s) ds \approx Q_{GL}^n = \sum_{i=0}^{n-1} w_i f(x_i), \quad (4.4)$$

for some nodes $\{x_i\}_{i=0}^{n-1}$ and weights $\{w_i\}_{i=0}^{n-1}$ with $n \in \mathbb{N}$, $n \geq 1$. In the previous expression ω is a given positive integrable weight function, supposed to be constant for the particular case of Gauss-Legendre quadrature. Gauss quadrature rules are exact [31] for any polynomial of degree $2n - 1$ or less, for a unique choice of nodes

$\{x_i\}$ and weights $\{w_i\}$. For the Gauss-Legendre rule, the nodes correspond to the roots of Legendre polynomials. There is no closed form expression for these and they are therefore computed to double precision using Newton-Raphson iterations [15, 27]

$$x_i^{(k+1)} = x_i^{(k)} - \frac{P_{n-1}(x_i^{(k)})}{P'_{n-1}(x_i^{(k)})}, \quad k > 1, \quad i = 0, \dots, n-1, \quad (4.5)$$

where P_{n-1} is the Legendre polynomial of degree $n-1$ which is computed by the three-term recurrence relation [26, Section 18.9(i)],

$$(n+1) P_{n+1}(x) = (2n+1)x P_n(x) - n P_{n-1}(x), \quad n \geq 1, \quad (4.6)$$

with the first two terms given by

$$P_0(x) = 1, \quad P_1(x) = x. \quad (4.7)$$

The first derivative is computed using [26, Section 14.10],

$$P'_{n+1}(x) = \frac{n}{x^2-1} x P_n(x) - P_{n-1}(x), \quad n \geq 1. \quad (4.8)$$

The initial guesses $\{x_i^{(0)}\}$ are given by a low order asymptotic approximation [15, 27]

$$x_i^{(0)} = \cos\left(\frac{4i+3}{4n+2}\pi\right), \quad i = 0, \dots, n-1. \quad (4.9)$$

The weights $\{w_i\}$ are then computed using [31]

$$w_i = \frac{2}{(1-x_i^2)(P'_{n-1}(x_i))^2}. \quad (4.10)$$

4.3 Highly oscillatory quadrature

There are numerous methods for efficiently evaluating oscillatory integrals. Here we focus on Filon quadrature rules [8, 18, 20], in which one approximates the modulating amplitude of the oscillations by a polynomial, and then integrates exactly. Other methods include the numerical method of steepest descent, which is based on a deformation of the path of integration into the complex plane to replace the oscillatory integrals by two Laplace-type integrals; see for instance [19].

We now describe the Filon-type method for evaluating the general integral

$$I_k^{[a,b]}[f] = \int_a^b f(s) e^{\pm iks} ds, \quad (4.11)$$

where $a, b, k \in \mathbb{R}$, with $a < b$ and $k > 0$. The function $f : [a, b] \rightarrow \mathbb{C}$ is supposed analytic. The case where a singularity is present in the domain is presented in the next section. Choose q points $a \leq x_1, \dots, x_q \leq b$ in (a, b) with respective multiplicity $m_1, \dots, m_q \in \mathbb{N}$. Let \tilde{f} be the unique Hermite interpolation polynomial of degree $m = \sum_{i=1}^q (m_i) - 1$ such that [20]

$$\tilde{f}^{(j)}(x_i) = f^{(j)}(x_i), \quad j = 0, \dots, m_i - 1, \quad 1, \dots, q. \quad (4.12)$$

Then the integral $I^{[a,b]}[f]$ is approximated by the quadrature rule

$$Q_F^{m+1}[f] = \int_a^b \tilde{f}(s) e^{\pm iks} ds, \quad (4.13)$$

which can be computed exactly provided that the so called moments $\mu_q = Q_F^{m+1}[P_q]$, where P_q is a polynomial of degree q of the interpolation basis, can themselves be computed exactly. The oscillator is here assumed linear $\pm iks$, hence the computation of the moments will be exact. This is not true for more general oscillators, even though, in some cases, a change of variables in the integral can be made to get a linear phase and a modified amplitude. The Filon method can then be applied directly. There also exist moment-free methods, see [18] for instance.

In particular, if the Legendre basis is used for the Hermite interpolation, which is the basis used in this work, the moments are computed as follows. By integration by parts, we have, for $n \geq 1$,

$$\mu_n = \int_a^b P_n(s) e^{\pm iks} ds, \quad (4.14)$$

$$= \mp \frac{i}{k} (P_n(b) e^{\pm ikb} - P_n(a) e^{\pm ika}) \pm \frac{i}{k} \int_a^b P'_n(s) e^{\pm iks} ds. \quad (4.15)$$

Now using the result [26, Section 14.10],

$$(2n+1)P_n = P'_{n+1} - P'_{n-1}, \quad n \geq 1, \quad (4.16)$$

we obtain the following recurrence relation to compute iteratively the moments

$$\mu_{n+1} = \mu_{n-1} + i \frac{2n+1}{k} \mu_n, \quad n \geq 1, \quad (4.17)$$

with the first two terms simply given by

$$\mu_0 = \mp \frac{i}{k} (e^{\pm ikb} - e^{\pm ika}), \quad \mu_1 = \mp \frac{i}{k} (be^{\pm ikb} - ae^{\pm ika}) + \frac{1}{k^2} (e^{\pm ikb} - e^{\pm ika}). \quad (4.18)$$

However, in practice, the sequence computed using the relation above diverges due to numerical errors for values of the wave number k inferior to the degree n . In this

situation, the domain of integration is subdivided in intervals of length equal to the wave length $\lambda = 2\pi/k$ and a standard high-order Gauss-Legendre quadrature rule is applied on each one. The moments are computed iteratively when k is larger than n (which is almost always the case in our numerical experiments). This is the only time the wave number appears explicitly in the numerical quadrature routines. Some convergence results of Filon-type quadrature rules are given in [24].

4.4 Treatment of singularities

Here we consider the case where a singularity is present at one end of the domain of integration. It is always possible to get to this situation by splitting the domain in two parts. Let $l \in \mathbb{R}$ with $l > 0$. Suppose that we have to evaluate the integral

$$J[l] = \int_0^l f(s)ds, \quad (4.19)$$

for which the integrand $f : [0, l] \rightarrow \mathbb{C}$ has a singularity at the origin $s = 0$. The singularity is dealt with by subdividing the interval of integration according to a geometrical grading towards the singularity and using n_g layers as follows. Construct the sequence $\{l_i\}_{i=0}^{n_g}$ such that

$$l_0 = 0, \quad l_i = \sigma^{n_g - i}, \quad i = 1, \dots, n_g. \quad (4.20)$$

The grading parameter σ is again here chosen to be equal to $\sigma = 0.15$. A quadrature rule is then applied on each sub-interval (l_{i-1}, l_i) for $i = 1, \dots, n_g$. A Filon-type quadrature as described in Section 4.3 is used if the integral $J[l]$ is oscillatory; a standard Gauss-Legendre quadrature as presented in Section 4.2 is used otherwise.

We remark that some singularities might be outside the domain of integration but still close to one end. If not dealt with properly, these near-singularities can be the source of numerical errors. Using a single element and applying the quadrature rules as in Sections 4.2 and 4.3 will not succeed in capturing the 'near-singularity' to the desired precision. One needs a strategy as the one described for a singular integral, involving some grading towards the 'near-singularity'. The approach proposed in this case is fairly simple but succeeds in computing the integrals to the desired precision. Let $l, d \in \mathbb{R}$ with $l > 0$ and $d > 0$. Suppose that we have to evaluate the integral

$$K[l, d] = \int_0^l f(s)ds, \quad (4.21)$$

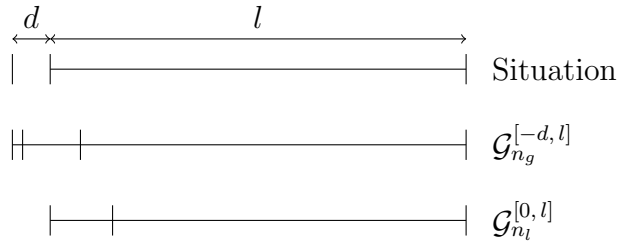


Figure 4.1: Sketch of the near-singularities strategy for which we have $n_l = 2$.

for which the integrand $f : [-d, l] \rightarrow \mathbb{C}$ has a singularity at $s = -d$. The procedure is as follows. For ease of implementation a geometrical mesh as above is used on the interval $(0, l)$ but with a reduced number of layers that we now determine. We consider the geometrical mesh $\mathcal{G}_{n_g}^{[-d, l]} = \{x_i\}_{i=0}^{n_g}$ as if the domain of integration was $[-d, l]$ with the associated number of layers n_g that would be used. Then the actual number of layers n_l used in the geometrical mesh $\mathcal{G}_{n_l}^{[0, l]}$ is computed as

$$n_l := \text{card} \left\{ x_i \in \mathcal{G}_{n_g}^{[-d, l]} \mid 0 < x_i \leq l \right\}. \quad (4.22)$$

From this definition, n_l is equivalently found from this definition as the only integer satisfying

$$\sigma^{n_l} \leq \frac{d}{l+d} \leq \sigma^{n_l-1}, \quad (4.23)$$

which finally yields the following explicit expression

$$n_l = \left\lceil \frac{\log \frac{l+d}{d}}{-\log \sigma} \right\rceil. \quad (4.24)$$

The number of layers required is computed in practical implementation as the formula above. The integral $K[l, d]$ in (4.21) is finally computed using a subdivision of the domain of integration according to the geometrical mesh $\mathcal{G}_{n_l}^{[0, l]}$. A sketch of the procedure is given in Figure 4.1.

4.5 Calibration of the numerical quadrature routines

The quadrature rules we described above have some parameters embedded which we shall now choose for our purposes. Note that this step could have been avoided by implementing adaptive versions of the quadrature rules. The choice of not using adaptive quadrature is justified by the fact that all the integral evaluations required

by the method to form the linear system (3.22), hence solve the problem, share the same form given by (4.2). The integrand of the integrals is well-known so that we are able to set the parameters in the quadrature rules once for all, therefore saving computational time.

This tuning of the parameters essentially amounts to select the number of quadrature nodes to obtain the aimed accuracy. Specifically, we aim at evaluating the integral (4.2) to the safe relative accuracy of $\approx 10^{-12}$. Recall that the integral (4.2) can be of four main 'types' for which we need to select the parameters: non-oscillatory non-singular, computed using Gauss-Legendre quadrature; non-oscillatory singular, computed using Gauss-Legendre quadrature on a geometrical mesh; oscillatory non-singular, computed using Filon quadrature; and oscillatory singular, computed using Filon quadrature on a geometrical mesh. The parameters for the 'near-singular' integrals are set to be equal to the parameters chosen for the singular integrals.

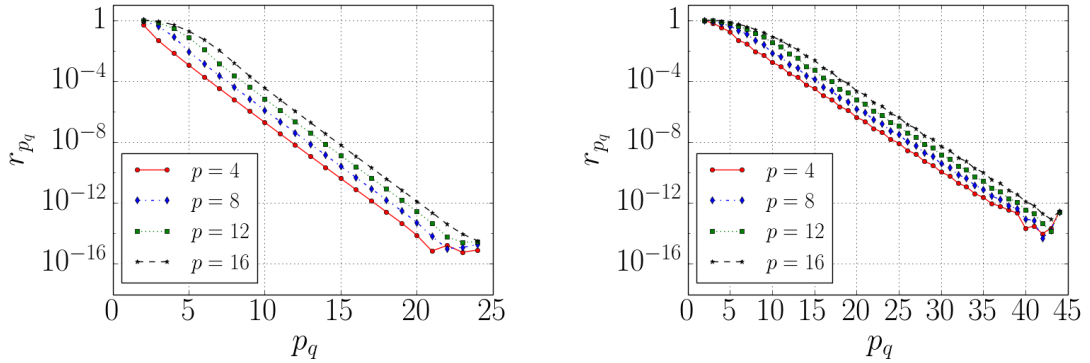
In our numerical experiments given in Chapter 5, we do not consider maximum polynomial degree p in (3.6) and (3.7) higher than $p = 16$. In the integral (4.2), the polynomial f has therefore in practice a degree lower or equal to $p = 16$. The numerical experimentations for tuning the quadrature parameters and reported thereafter are obtained in the special case where $(a, b) = (0, 1)$ in (4.2) and with a wave number $k = 10^6$. The position of the singularity is given by $x = -0.18$ in the non-singular case, which is close to the limit ≈ 0.17647 for which the integral is classified as 'near-singular'. The singular case presented corresponds to the situation where $x = 0$. In the singular or non-singular case, the integral is oscillatory when $\theta = 1$ and non-oscillatory when $\theta = -1$. Other numerical experimentations than the ones presented thereafter were performed to check the robustness of the choices made, in particular with respect to the wave number k but also the integral bounds and position of the singularity. The convergence results we now present illustrate the tuning, confirmed by numerous other results.

We start by the Gauss-Legendre quadrature rule described in Section 4.2 and for which we need to determine the order of the quadrature, denoted n_{GL} , so as to evaluate non-oscillatory non-singular integrals of the form of (4.2) to the desired precision. To do so, we compute the relative error r_{p_q} such that

$$r_{p_q} := \frac{|Q_{GL}^{p_q} - Q_{GL}^*|}{|Q_{GL}^*|}, \quad (4.25)$$

where $Q_{GL}^{p_q}$ is defined in (4.4) and Q_{GL}^* is taken as a reference value of the integral, computed with a high order Gauss-Legendre quadrature rule. The convergence of

the relative error r_{p_q} with respect to the quadrature order p_q for different polynomial degree p of the polynomial f in (4.2) is given in Figure 4.2a. From these results and others, we choose $n_{GL} = 20$ quadrature nodes in the Gauss-Legendre quadrature rule (4.4) to compute non-oscillatory and non-singular integrals.



(a) Gauss-Legendre quadrature, non-singular integrand. (b) Filon quadrature, non-singular integrand.

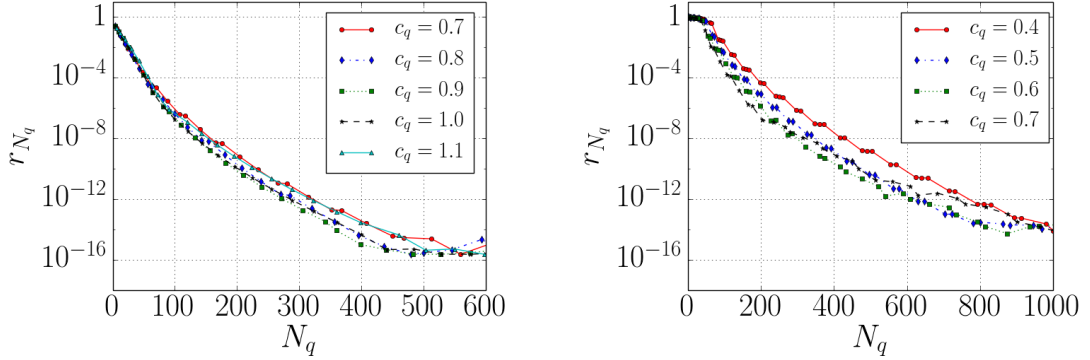
Figure 4.2: Convergence of the relative error r_{p_q} with respect to the order of the quadrature rule p_q for the computation of the non-singular integral (4.2) and for several different polynomial degrees p of the polynomial f using Gauss-Legendre (left) and Filon (right) quadrature rules.

We turn now to the Filon quadrature rule described in Section 4.3 and for which we need to determine the order of the quadrature, denoted n_F , so as to evaluate oscillatory non-singular integrals of the form of (4.2) to the desired precision. To do so, we abuse notation and compute the relative error r_{p_q} such that

$$r_{p_q} := \frac{|Q_F^{p_q}[f] - Q_F^*[f]|}{|Q_F^*[f]|}, \quad (4.26)$$

where $Q_F^{p_q}[f]$ is defined in (4.13) and $Q_F^*[f]$ is taken as a reference value of the integral, computed with a high order Filon quadrature rule. The convergence of the relative error r_{p_q} with respect to the quadrature order p_q , for different polynomial degrees p of the polynomial f in (4.2), is given in Figure 4.2b. From these results and others, we choose $n_F = 40$ quadrature nodes in the Filon quadrature rule (4.13) to compute oscillatory and non-singular integrals.

We consider now singular integrals as described in Section 4.4. Recall that to capture the singularity, a geometrical mesh using n_g layers is constructed and a



(a) Gauss-Legendre quadrature, singular integrand. (b) Filon quadrature, singular integrand.

Figure 4.3: Convergence of the relative error r_{N_q} with respect to the number of quadrature nodes N_q for the computation of the singular integral (4.2) and for several values of the parameter c_q using Gauss-Legendre (left) and Filon (right) quadrature rules. The polynomial degree p of the polynomial f is $p = 16$.

Gauss-Legendre or Filon quadrature rule is applied to each subinterval of this mesh, depending on the oscillatory nature of the integrand. The order of the quadrature applied to each of the subinterval, denoted p_q , is assumed constant. Given p_q , the number of layers n_g used in the construction of the geometrical mesh is computed as $n_g = \lceil c_q(p_q + 1) \rceil$, where c_q is a parameter that we need to determine. The tuning of p_q and c_q is done in order to minimise the number of quadrature nodes used, denoted N_q , and such that $N_q := n_g(p_q + 1) = c_q(p_q + 1)^2$. Let $Q_{GL}^{c_q, p_q}$ be the quadrature rule for non-oscillatory singular integrals and $Q_F^{c_q, p_q}$ be the quadrature rule in the oscillatory case. The optimal values of the parameters c_q and p_q for the singular quadrature with respectively Gauss-Legendre and Filon quadrature on the subintervals are denoted by c_q^{GL} , n_{GL}^s and c_q^F , n_F^s . To choose these parameters, we compute the relative error r_{N_q} such that

$$r_{N_q} := \frac{|Q_T^{c_q, p_q} - Q_T^*|}{|Q_T^*|}, \quad (4.27)$$

where T is either GL or F and Q_T^* is a reference value for the integral computed with the corresponding high order quadrature rule. The convergence of the relative error r_{N_q} with respect to the number of quadrature nodes N_q is given in Figure 4.3. From these results and others, we choose $c_q^{GL} = 1$, $n_{GL}^s = 17$ for the computation of non-oscillatory singular integrals and we choose $c_q^F = 1/2$, $n_F^s = 34$ in the oscillatory case. Note that the choices of c_q are not optimal with respect to the results

presented, but a slight k -dependency on the optimal value for the parameter c_q has been observed. The values selected ensure that the aimed accuracy is obtained for all integrals encountered. Note also that these choices imply that the same number of layers $n_g = 18$ is used, whether the integral is oscillatory or not.

Chapter 5

Numerical results

5.1 Comparison of the different approximation strategies

The implementation of the HNA BEM was coded in PYTHON, with the exception of the quadrature routines for which C++ was preferred for efficiency reasons. The Filon quadrature routines were based on MATLAB codes kindly supplied by Dr Stephen LANGDON (University of Reading).

Different approximation strategies were presented in Chapter 3 and we now compare their performance. To simplify the discussion, we introduce the following convenient notations. The HNA BEM using an approximation space based on one single mesh is further referred to as the M^s method, whereas the related HNA BEM using the approximation space based on two overlapping meshes is referred to as the M^o method. For each of these two methods, the allocation of the collocation points locally on each mesh elements can be done using either a uniform distribution of the collocations points according to (3.23), for which the subscript u is used, or a Chebyshev distribution of the collocations points according to (3.24), for which the subscript C is used. Accordingly, we refer to the four different strategies as the M_u^s , M_C^s , M_u^o and M_C^o methods.

Let $p \in \mathbb{N}$ be the maximum degree of the polynomials in the approximation space \mathcal{S}_N . We adopt an hp -strategy, namely we increase the number of elements in the meshes together with p to obtain better accuracy of the solution. The relation between the number of elements n_i^\pm in the meshes and the maximum polynomial degree p is as follows. We take for $i = 1, \dots, n_s$,

$$n_i^+ = n_i^- = \max(2, \lfloor c_L(p+1) \rfloor), \quad (5.1)$$

where $c_L \in \mathbb{R}$, $c_L > 0$, is a parameter. We usually take $c_L = 2$ in our numerical experiments but other alternatives are considered thereafter. The choice of using at least two layers is imposed by the overlapping meshing strategy in order to avoid singular matrix. We choose in addition $\alpha = 1$ in the definitions of the vectors of degrees \mathbf{p}_i^\pm in (3.6) and (3.7), although other alternatives for α are also considered thereafter.

The comparison of the different methods is done on a simple test case consisting of one single screen $\Gamma = \Gamma_1$ with $L = 1$ so that $(s_1, s_2) = (0, 1)$. We consider an oblique incident plane wave u^i in (2.1) with $\mathbf{d} = (1/\sqrt{2}, -1/\sqrt{2})$.

We abuse notation and denote in the plots the numerical solution as φ_p using the more meaningful polynomial degree p as subscript rather than the total number of degrees of freedom N . The solution $|\varphi_p|$ with $p = 8$ on the screen Γ_1 for two wave numbers $k = 16$ and $k = 256$ is given in Figure 5.1. Note the logarithmic scale used and the discontinuities in the numerical approximations. The real part of the total field $u = u^i + u^s$ in the domain D for $k = 16$ is represented in Figure 5.2. The M_u^o method is used for plotting purposes.

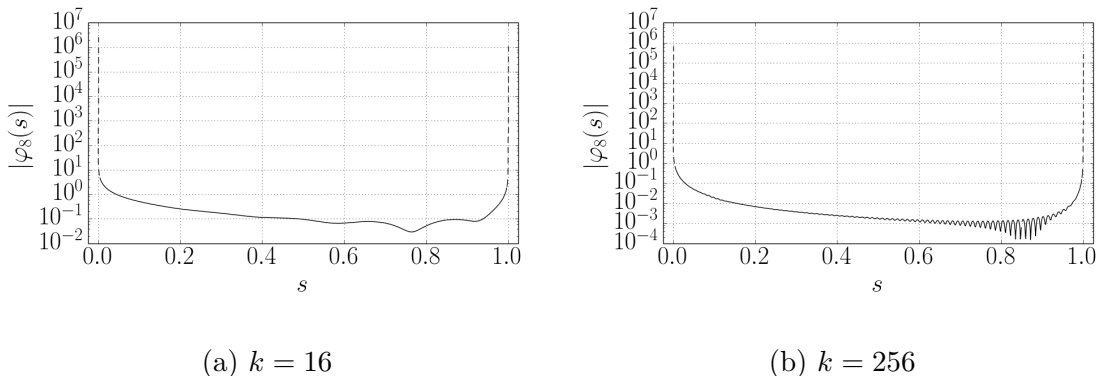


Figure 5.1: Solution $|\varphi_p|$ with $p = 8$ on the screen Γ_1 for two frequencies $k = 16$ and $k = 256$ and for an incidence $\mathbf{d} = (1/\sqrt{2}, -1/\sqrt{2})$.

We now study the convergence of the approximate solution φ_N to the exact solution φ on the screens Γ . No analytical solution is available to compare with. For moderate frequencies $k < 300$, we use as reference the numerical solution computed using a spectral method from the `SingularIntegralEquations.jl` JULIA package [29], noted ϕ_{SIE} and computed to machine precision on the screen. Note that the output solution ϕ_{SIE} corresponds to the total jump on the screen, namely $[\frac{\partial u}{\partial n}]$ as in (2.20). We therefore compare it to $\phi_N := \Psi + k\varphi_N$ from our numerical solution.

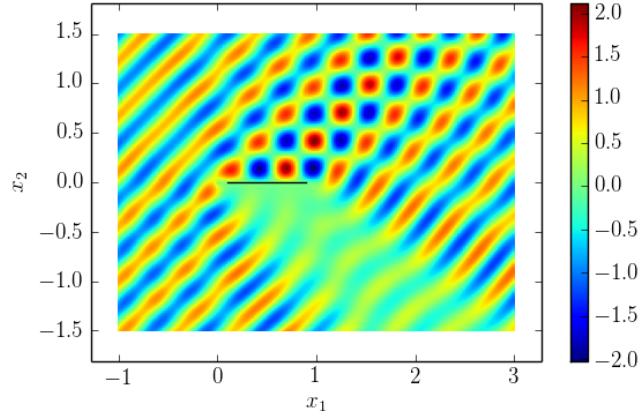


Figure 5.2: Real part of the total field $u = u^i + u^s$ in the domain D for the scattering problem with one screen Γ_1 , wave number $k = 16$ and incidence $\mathbf{d} = (1/\sqrt{2}, -1/\sqrt{2})$.

Our approximate solution φ_N is in $\tilde{H}^{-1/2}(\Gamma)$. As a result, convergence of the approximate solution should be presented in the associated norm $\|\cdot\|_{\tilde{H}^{-1/2}(\Gamma)}$, defined precisely in [9, 23]. This norm is however difficult to evaluate numerically. Following [16], a possibility is to compute $\|\cdot\|_{\Gamma}$ defined as

$$\|\phi\|_{\Gamma} := \sqrt{|\langle S_k \phi, \phi \rangle|}, \quad \phi \in \tilde{H}^{-1/2}(\Gamma), \quad (5.2)$$

which is an equivalent norm on $\tilde{H}^{-1/2}(\Gamma)$ and is easier to compute [16]. Note that this norm still requires the evaluation of a double integral. We therefore prefer to use a computationally cheaper norm, namely the norm on the $L^q(\Gamma)$ space, noted $\|\cdot\|_{L^q(\mathbb{R})}$, with $q = 3/2$ such that

$$\|\phi\|_{L^q(\mathbb{R})} = \left(\int_{\Gamma} |\phi(s)|^q ds \right)^{1/q}, \quad \phi \in L^q(\Gamma). \quad (5.3)$$

This choice directly follows from the result given in Corollary 5.4 in [16] that we quote now.

Theorem 5.1. *For $1 < q \leq 2$, $L^q(\mathbb{R})$ can be continuously embedded in $H^{-1/2}(\mathbb{R})$ with*

$$\|\phi\|_{H_k^{-1/2}(\mathbb{R})} \leq k^{1/q-1} \max \left[1, \frac{1}{\sqrt{(2\pi-1)(q-1)}} \right] \|\phi\|_{L^q(\mathbb{R})}, \quad \phi \in L^q(\mathbb{R}). \quad (5.4)$$

The above result implies that the $L^q(\Gamma)$ norm for $1 < q \leq 2$ is stronger than the $H_k^{-1/2}(\Gamma)$ norm, which defines an equivalent norm on $\tilde{H}^{-1/2}(\Gamma)$; see [9, Section 2.] for precise definitions and properties of these norms. Therefore, convergence in $\|\cdot\|_{L^q(\Gamma)}$

implies convergence in the appropriate space $\tilde{H}^{-1/2}(\Gamma)$. Even though the numerical approximation is in $L^q(\Gamma)$ for $q \geq 1$, the exact solution is not in $L^2(\Gamma)$ (see the remark following Theorem 2.1). The choice of the $L^{3/2}(\Gamma)$ norm has therefore been made. Note that no particular physical meaning is associated with this norm but it fits our purposes.

In practice, the numerical evaluation of the $L^{3/2}(\Gamma)$ norm still requires much care as the integrand typically exhibits high absolute values near the corners of the screens as well as high oscillations. The oscillations are captured by subdividing the domain of integration into subintervals with length of the order of the wavelength. The singularities near the domain ends are tackled as before by introducing subdivisions of the domain of integration according to a geometrical grading towards the corners. On each subinterval a high-order Gauss-Legendre quadrature rule is applied.

We compute the relative error $r_p[\phi_p]$ for the polynomial degree p , defined as

$$r_p[\phi_p] := \frac{\|\phi_{\text{SIE}} - \phi_p\|_{L^{3/2}(\Gamma)}}{\|\phi_{\text{SIE}}\|_{L^{3/2}(\Gamma)}}. \quad (5.5)$$

The convergence plots of the relative errors $r_p[\phi_p]$ for the M_u^s and M_u^o methods is given in Figure 5.3.

When achieved, the convergence with respect to the polynomial degree p is exponential. This was expected from the results presented for the Galerkin method in [16], and our best approximation result in Theorem 3.1 (for the overlapping meshing strategy). Even though we lack a quasi-optimality estimate, contrary to the Galerkin method, these results hint at the possibility that a similar result could hold for the collocation method.

Another remarkable feature of these convergence plots is the decrease of the error for a given polynomial degree p as the wave number of the problem k increases, reproducing the results in [16] for the Galerkin scheme. This suggests that the performance of the HNA method actually improves with the frequency, assuming that the reference solution is computed to the same precision uniformly in k .

For some particular frequencies, the convergence of the error is either not obtained (low frequencies in the overlapping meshes case) or not exponential (relatively high frequencies in the single mesh case). A closer look to the numerical solutions shows that they exhibit spurious oscillations. These oscillations are present at the ends of the mesh elements in the centre of the screen, in the single mesh case. In the overlapping meshes case, however, the oscillations are present in the small elements near the corners of the screen. We note similarities of these oscillations with the Runge

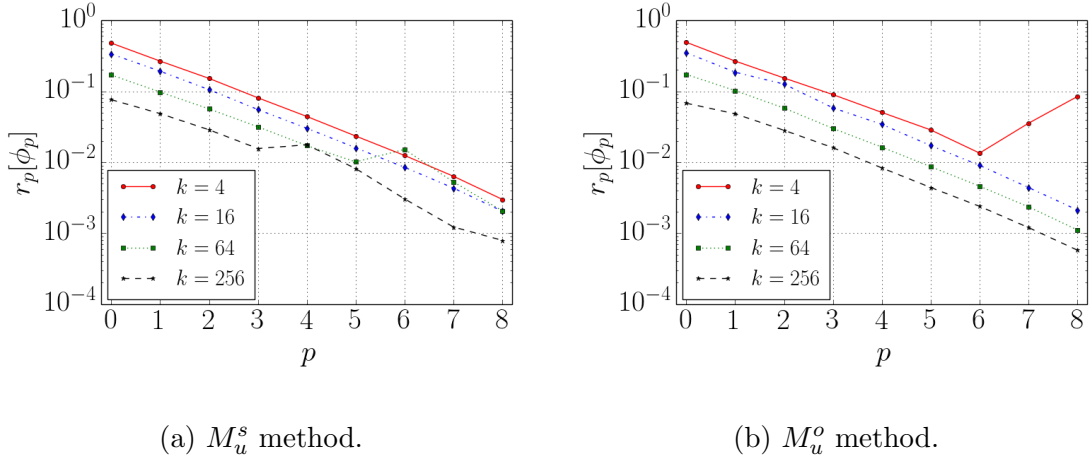


Figure 5.3: Comparison of the convergence of the relative error $r_p[\phi_p]$ on the boundary with respect to the polynomial degree p for several frequencies and the two meshing strategies. Uniform allocation of the collocation points locally on each mesh elements. Scattering problem with one screen Γ_1 and with incidence $\mathbf{d} = (1/\sqrt{2}, -1/\sqrt{2})$.

phenomenon, at least in the case of the single type mesh, as they are located at the end of the element supporting the polynomial, and manifest themselves particularly when the polynomial order increases. The uniform allocation of the collocation points locally on each mesh elements according to (3.23) is then reconsidered. The other allocation process, using a Chebyshev distribution of the collocation points locally on each elements according to (3.24), is now tested. The convergence plots of the relative errors $r_p[\phi_p]$ for the two methods M_C^s and M_C^o using this Chebyshev distribution of collocation points is given in Figure 5.4. The improvement of the convergence of the error for the M_C^s method is clear, as exponential convergence is achieved for all frequencies. For the M_C^o strategy, however, the convergence of the error is clearly harmed for $p \geq 4$. In fact the solutions are now wrong, except for $k = 256$ for which we obtain convergence, although not exponentially.

To further investigate this issue, we first plot the evolution of the condition number, noted κ_p , of the matrix \mathbf{M} of the linear system (3.22) with respect to the maximal polynomial degree p ; see Figure 5.5. For all methods the growth of the condition number κ_p is exponential with respect to the polynomial degree p . In fact, no real difference in the conditioning is observed between the different methods, quite surprisingly. The fact that the growth seems bounded by 10^{17} is likely due to a wrong numerical evaluation of κ_p when these high values are reached.

The rate of increase is noticeably more important for small wave numbers. For

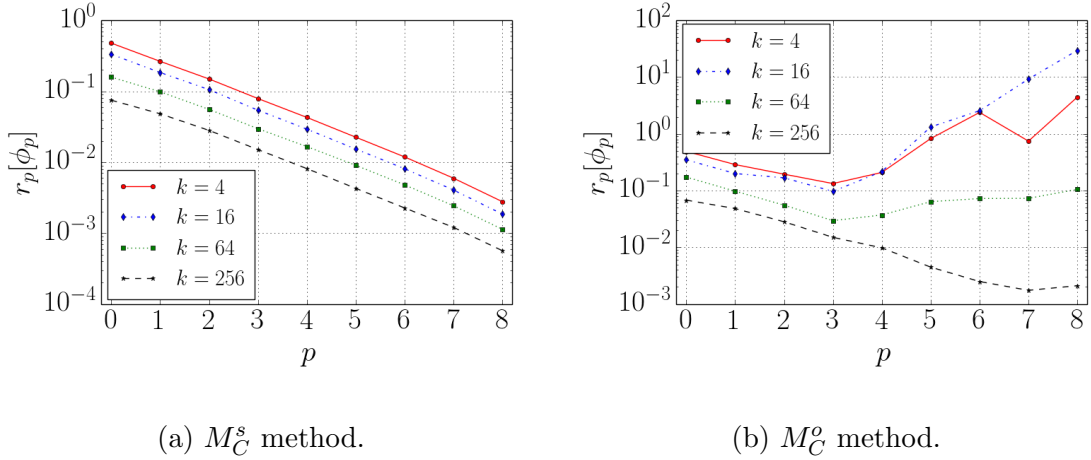


Figure 5.4: Comparison of the convergence of the relative error $r_p[\phi_p]$ on the boundary with respect to the polynomial degree p for several frequencies and the two meshing strategies with allocation of the collocation points on Chebyshev grids locally on each mesh elements. Scattering problem with one screen Γ_1 and with incidence $\mathbf{d} = (1/\sqrt{2}, -1/\sqrt{2})$.

moderate to large values of k , note also the slight decrease in the condition number as k increases. This was expected since the two oscillatory terms in φ exhibit similar behaviour when the wavelength λ is of the order of the length of the screen. The direct solver used to solve the linear system can however in this case produce inaccurate results. The bad conditioning of the matrix \mathbf{M} could therefore explain the poor convergence observed for small frequencies for the M_u^o method in Figure 5.3b.

As discussed previously in Section 3.3 and pointed out in [2], the conditioning of the problem in the overlapping meshing strategy could be possibly improved by preventing two collocations points belonging to the two different meshes to be too close. This has not been tested and could be investigated in further work. However, the conditioning of the matrix \mathbf{M} alone cannot explain the lack of convergence for the M_C^o method displayed in Figure 5.4b. In this case, the current explanation might be that the implementation of this particular configuration is prone to numerical instability, further complicated by the ill-conditioning. It is possible that a different implementation using the same approximation space would provide different results for which convergence would be achieved. In the light of these results, it is unfortunately not possible to decide which meshing strategy is best.

The wave numbers considered so far are relatively moderate so that we are able to compare with the reference solution from the `SingularIntegralEquations.jl`

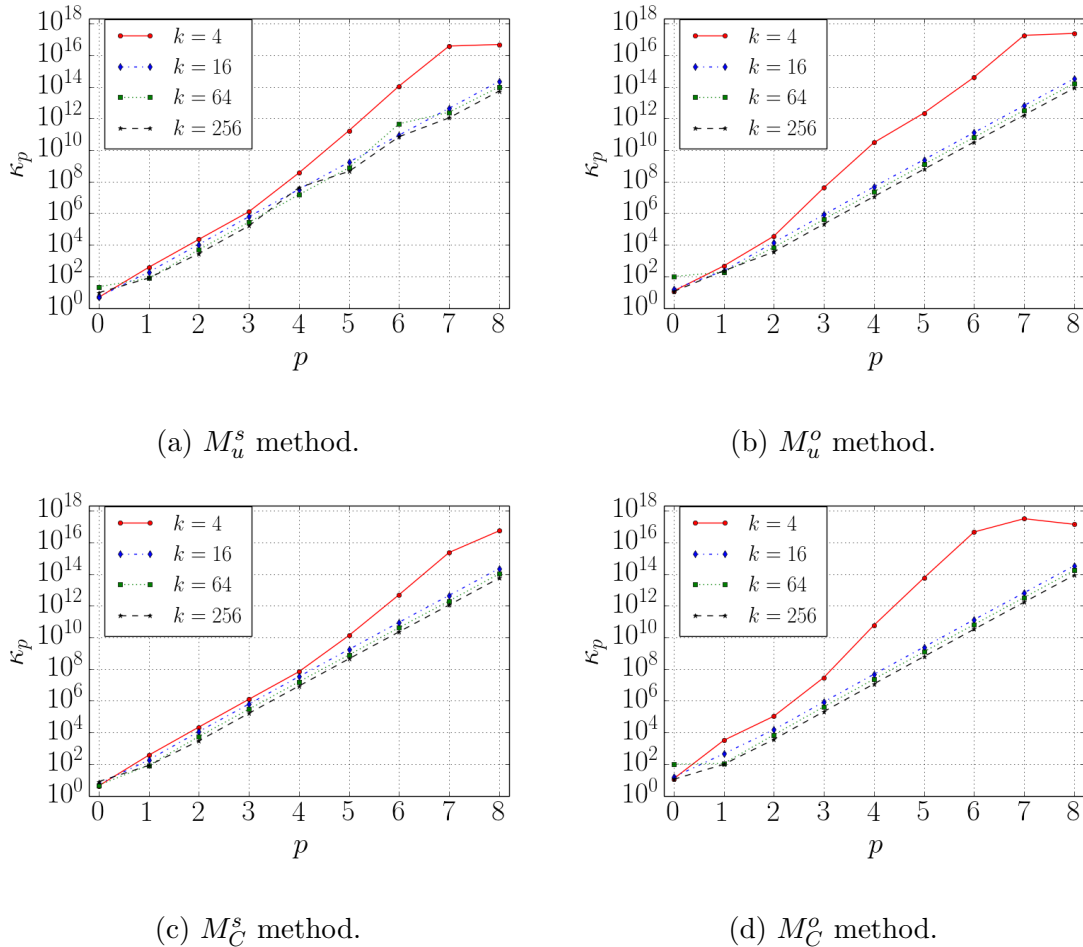


Figure 5.5: Comparison of the condition number κ_p of the matrix \mathbf{M} with respect to the polynomial degree p for several frequencies. Scattering problem with one screen Γ_1 and with incidence $\mathbf{d} = (1/\sqrt{2}, -1/\sqrt{2})$.

JULIA package. We now show convergence of the method for much larger frequencies by computing an alternative relative error $\tilde{r}_p[\phi_p]$ again with respect to the polynomial degree p but using ϕ_8 as a reference solution (when actual convergence is achieved) and considering only $p < 8$

$$\tilde{r}_p[\phi_p] := \frac{\|\phi_8 - \phi_p\|_{L^{3/2}(\Gamma)}}{\|\phi_8\|_{L^{3/2}(\Gamma)}}. \quad (5.6)$$

The convergence of the error $\tilde{r}_p[\phi_p]$ for all four methods is given in Figure 5.6. The error $r_p[\phi_p]$, rather than $\tilde{r}_p[\phi_p]$, has already been computed for the two smaller wave numbers $k = 16$ and $k = 256$ and therefore serves as a comparison. These new results at large frequencies confirm the exponential convergence with respect to the polynomial degree p when using either the M_C^s or the M_u^o strategies. The lack of

convergence of the M_u^s at large frequencies is also confirmed, as no convergence has been achieved for $k = 65536$. The somewhat surprising result is the exponential convergence of the M_C^o strategy for large frequencies.

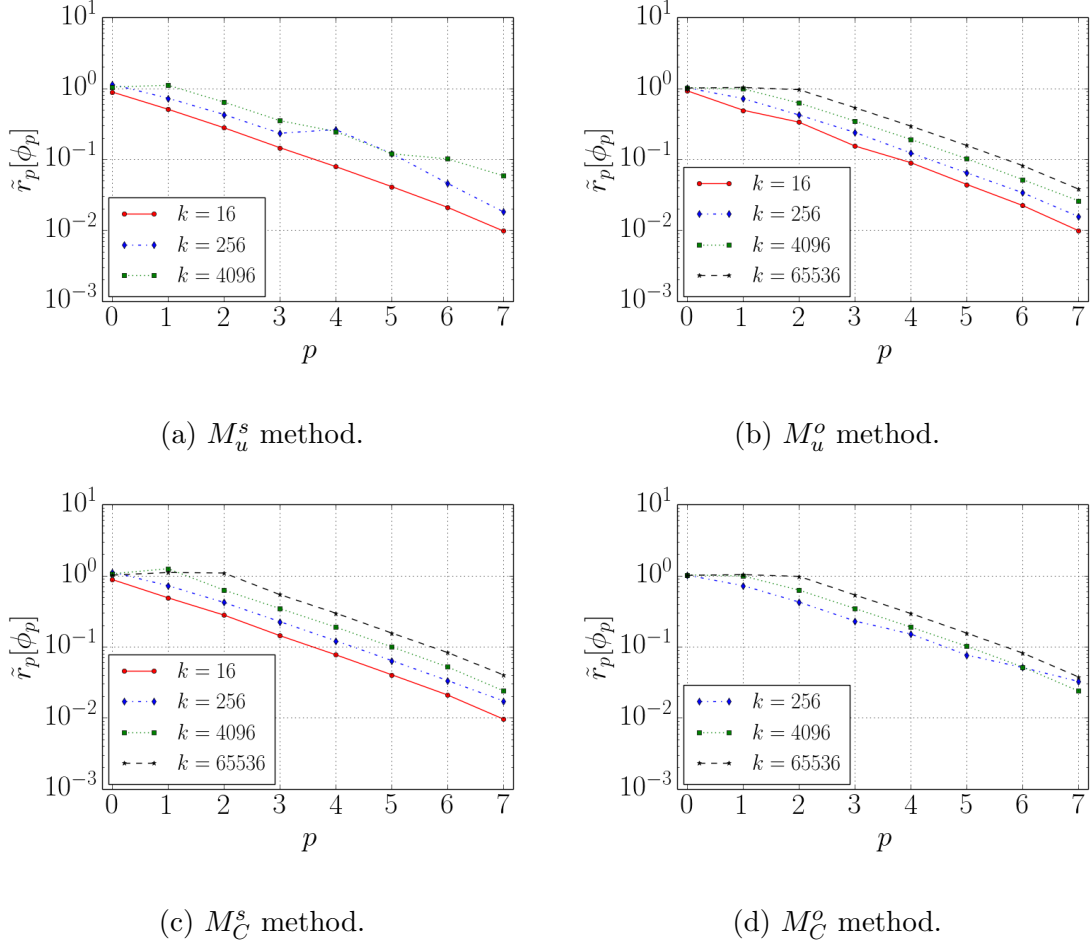


Figure 5.6: Comparison of the convergence of the relative error $\tilde{r}_p[\phi_p]$ on the boundary with respect to the polynomial degree p for several frequencies. Scattering problem with one screen Γ_1 and with incidence $\mathbf{d} = (1/\sqrt{2}, -1/\sqrt{2})$.

To sum up the previous results exposed, the M_C^s method is the most effective as it converges for all frequencies tested; the M_u^o method performs really similarly, except at low frequencies where conditioning issues arise. Further results are therefore only presented for the two methods M_C^s and M_u^o .

We compare the convergence with respect to the number of degrees of freedom N of the method, in order to determine the most computationally efficient method. To do this, we use the reference solution from the `SingularIntegralEquations.jl` package and compute the relative error $r_N[\phi_N]$ with respect to the total number of

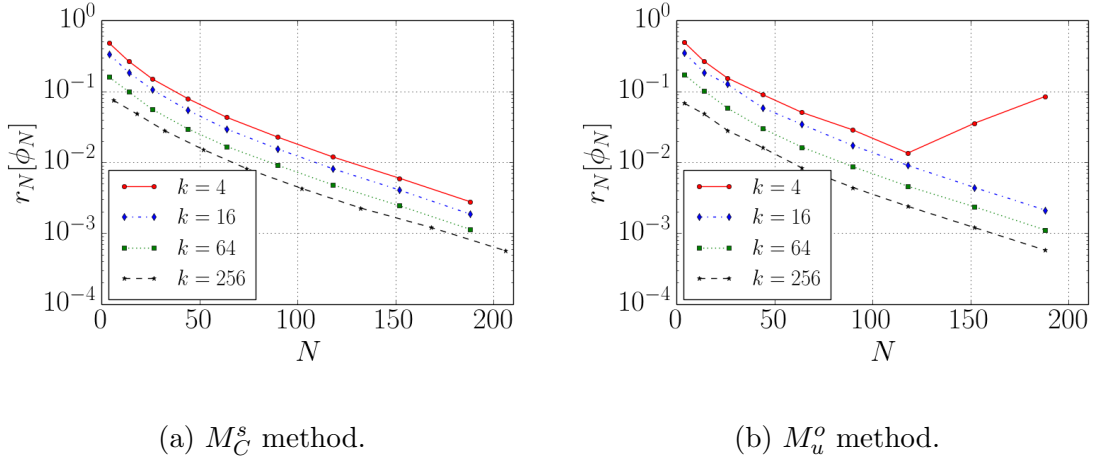


Figure 5.7: Comparison of the convergence of the relative error $r_N[\phi_N]$ on the boundary for several frequencies. Scattering problem with one screen Γ_1 and with incidence $\mathbf{d} = (1/\sqrt{2}, -1/\sqrt{2})$.

degrees of freedom N defined as

$$r_N[\phi_N] := \frac{\|\phi_{\text{SIE}} - \phi_N\|_{L^{3/2}(\Gamma)}}{\|\phi_{\text{SIE}}\|_{L^{3/2}(\Gamma)}}. \quad (5.7)$$

The convergence plots of the relative errors $r_N[\phi_N]$ are given in Figure 5.7. For small frequencies, the number of degrees of freedom N in both methods are identical for a given p . However, this does not hold for larger values of the frequency, for which the M_C^s strategy tends to add more degrees of freedom for similar levels of accuracy obtained. The M_u^o method is therefore expected to perform even more efficiently with respect to N as the frequency gets higher. Recall however that N for the M_C^s method is bounded uniformly with respect to k , so that the difference in performance for p fixed between the two strategies will stop increasing for a limiting value of k .

We now turn our attention to the choice of two parameters present in the approximation space, namely the parameter α used in the definitions of the vectors of degrees \mathbf{p}_i^\pm in (3.6) and (3.7), and the parameter c_L used in (5.1).

Starting with the parameter α , we plot the evolution of the error $r_N[\phi_N]$ with respect to the number of degrees of freedom N , together with the evolution of the condition number κ_p of the matrix \mathbf{M} with respect to the polynomial degree p , for different values of the parameter α , in Figure 5.8. From the graphs, it is clear that the choice $\alpha = 0$, corresponding to constant maximum polynomial degree on every mesh element, only increases slightly the accuracy of the method, at the cost of an important increase in the number of degrees of freedom used and in the conditioning

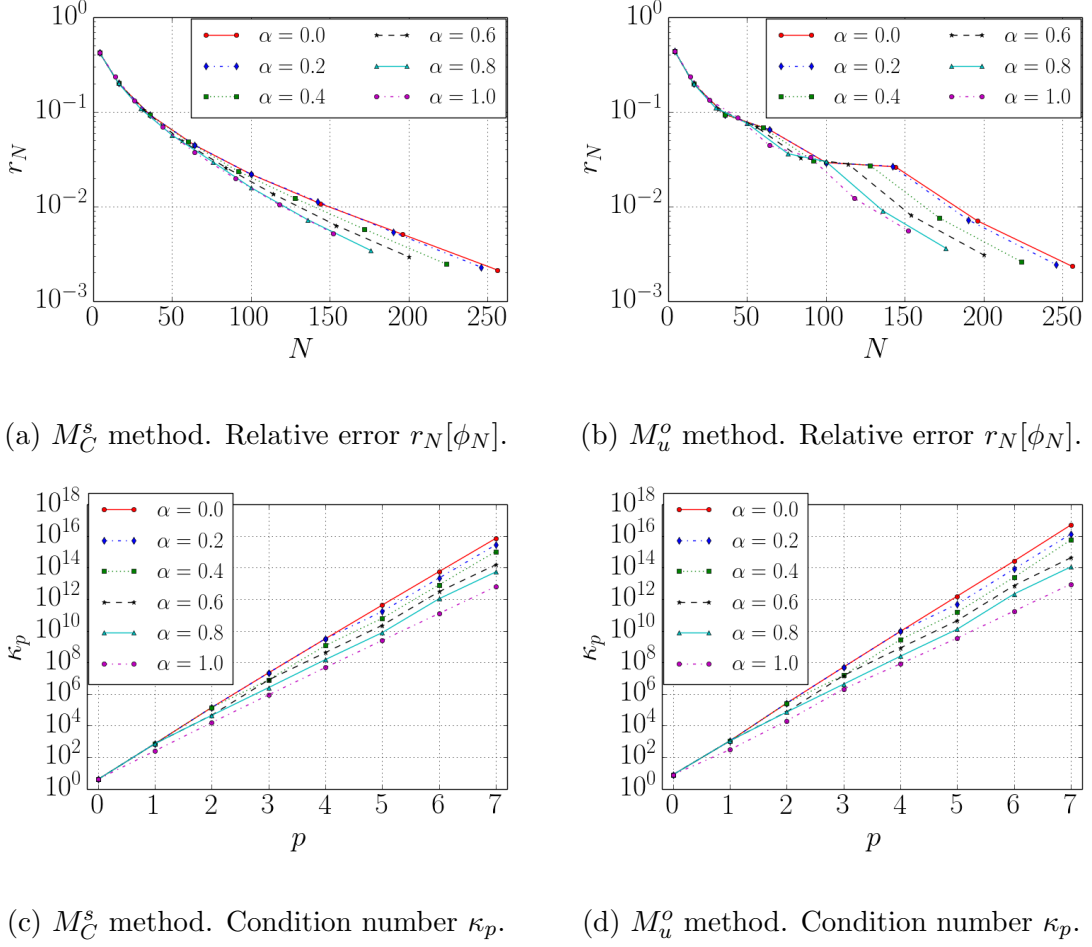
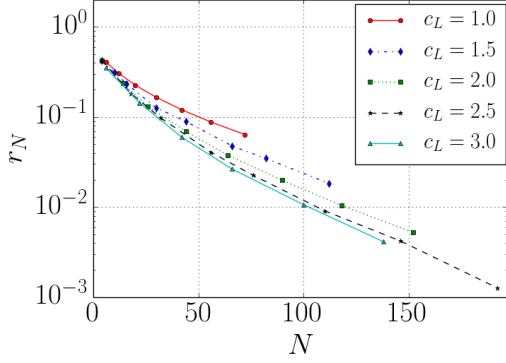


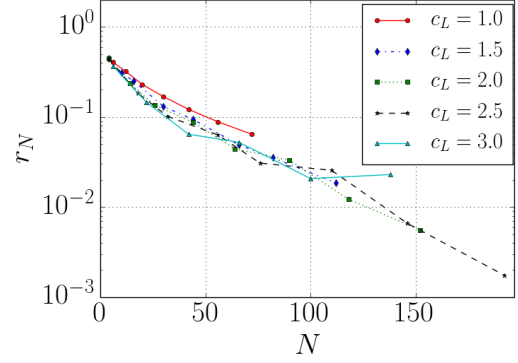
Figure 5.8: Comparison of the convergence of the relative error $r_N[\phi_N]$ on the boundary with respect to the number of degrees of freedom N , and of the evolution of the condition number κ_p of the matrix \mathbf{M} with respect to the polynomial degree p , for different values of the parameter α . Scattering problem with one screen Γ_1 , wave number $k = 8$ and incidence $\mathbf{d} = (1/\sqrt{2}, -1/\sqrt{2})$.

of the problem. The choice $\alpha = 1$, corresponding to a linear decrease in the maximal degree of the approximating polynomials gradually towards the singularities, is then legitimate.

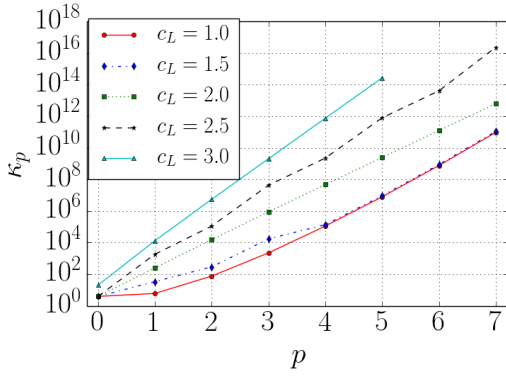
We now plot in Figure 5.9 the evolution of the error r_N with respect to the number of degrees of freedom N , and evolution of the condition number κ_p of the matrix \mathbf{M} with respect to the polynomial degree p , for different values of the second parameter of interest c_L . Note that for the case $c_L = 3$, the maximum polynomial degree considered is $p = 5$ compared to $p = 7$ for the other values. Higher values of p in this case ($c_L = 3$) leads to too much refinement in the geometrical meshes used. Indeed,



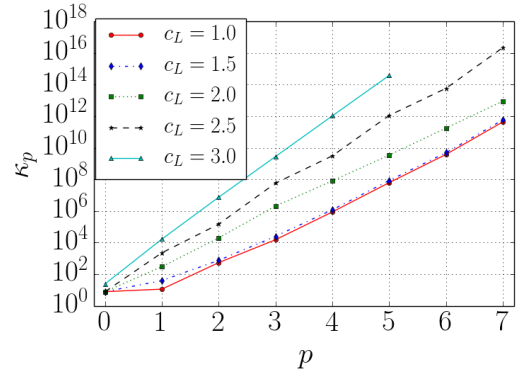
(a) M_C^s method. Relative error $r_N[\phi_N]$.



(b) M_u^o method. Relative error $r_N[\phi_N]$.



(c) M_C^s method. Condition number κ_p .



(d) M_u^o method. Condition number κ_p .

Figure 5.9: Comparison of the convergence of the relative error $r_N[\phi_N]$ on the boundary with respect to the number of degrees of freedom N , and of the evolution of the condition number κ_p of the matrix \mathbf{M} with respect to the polynomial degree p , for different values of the parameter c_L . Scattering problem with one screen Γ_1 , wave number $k = 8$ and incidence $\mathbf{d} = (1/\sqrt{2}, -1/\sqrt{2})$.

when using double precision, one cannot use more than 18 layers in a geometrical mesh with a grading parameter of $\sigma = 0.15$.

The improvement in the convergence of the error r_N with increasing values of the parameter c_L , hence increasing refinement in the geometrical grading of the meshes, demonstrates the efficiency of this approach to capture the singularities in the screen corners. However, using a too high value of c_L , such as $c_L \geq 3$, only allows to resolve the singularities, at the cost of a poor resolution of the oscillations. It also leads to ill-conditioning of the problem, that prevents to reach the desired accuracy by limiting the maximum polynomial degree p that can be used in the method. On the

contrary, using a too low value of c_L , such as $c_L \leq 1$, imposes to greatly increase the maximum polynomial degree p used in order to obtain a desired accuracy, which can also lead to ill-conditioning. The optimality seems therefore to lie in between, with values such as $c_L = 2$. For this choice of c_L , relatively fast convergence is obtained and the maximum polynomial degree p can be increased in order to obtain the desired level of accuracy.

We also highlight the fact that the $L^{3/2}(\Gamma)$ norm might measures preferentially the convergence in the capture of the singularities rather than in the capture of the oscillations. In this respect, the choice of the optimal values for the two parameters α and c_L might differ according to the norm used.

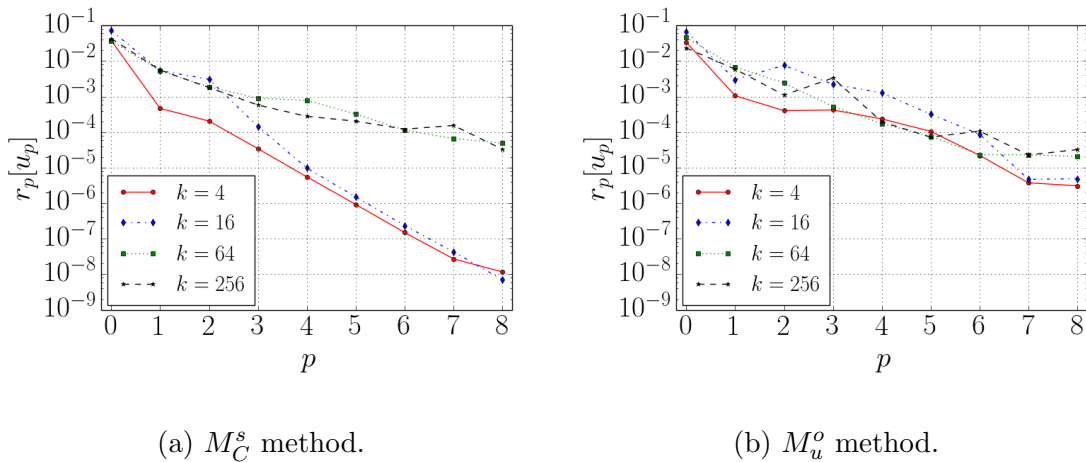


Figure 5.10: Comparison of the convergence of the relative error $r_p[u_p]$ in the domain of propagation D with respect to the polynomial degree p for several frequencies. Scattering problem with one screen Γ_1 and with incidence $\mathbf{d} = (1/\sqrt{2}, -1/\sqrt{2})$.

We now turn to the evaluation of another quantity of more physical interest, namely the value of the total field $u = u^i + u^s$ in the domain D of propagation. Following previous notation, we refer to the numerical approximation of the total field as u_p , where p denotes the maximum polynomial degree used. No theoretical error estimates are available for the total field approximation u_p . However, following the proof of Theorem 6.2 in [16], we remark that for $\mathbf{x} \in D$, we have

$$|u(\mathbf{x}) - u_p(\mathbf{x})| = k|\mathcal{S}_k(\varphi - \varphi_p)(\mathbf{x})|, \quad (5.8)$$

$$\leq k\|\Phi_k(\mathbf{x}, \cdot)\|_{H_k^{1/2}(\Gamma)}\|\varphi - \varphi_p\|_{\tilde{H}_k^{-1/2}(\Gamma)}. \quad (5.9)$$

The quantity $\|\Phi_k(\mathbf{x}, \cdot)\|_{H_k^{1/2}(\Gamma)}$ is bounded, although non uniformly, in D , with a k dependence behaving like $\mathcal{O}(\log^{1/2}(k))$; see Lemma 4.6(ii) in [16]. From our best-

approximation result in Theorem 3.1 and the exponential convergence of the numerical approximation φ_p on the boundary, one can expect that the numerical approximation of the wave field u_p converges also exponentially in the domain D .

The accuracy of the numerical approximation is investigated by approximating the infinity norm on a circle, noted C , of centre $(1/2, 0)$ and radius 1 in the domain. The reference solution, denoted u_{SIE} , is computed using the `SingularIntegralEquations.jl` JULIA package. We compute $r_p[u_p]$ defined as

$$r_p[u_p] := \frac{\max_{\mathbf{x} \in C} |u_p(\mathbf{x}) - u_{\text{SIE}}(\mathbf{x})|}{\max_{\mathbf{x} \in C} |u_{\text{SIE}}(\mathbf{x})|}, \quad (5.10)$$

on 2560 points uniformly distributed on the circle, so that there are 10 points per wavelength for the highest wave number considered $k = 256$. The convergence plots are given in Figure 5.10. While convergence of the numerical approximation u_p to the reference solution u_{SIE} is clearly obtained, it is not possible to assert that exponential convergence is achieved. For the M_C^s method, the somewhat better convergence rate that seems to be obtained at low frequencies could be explained by the fact that the oscillations are resolved not only by the explicit oscillatory factors $e^{\pm iks}$ in our approximation space, but also by the high order polynomials approximating the amplitudes.

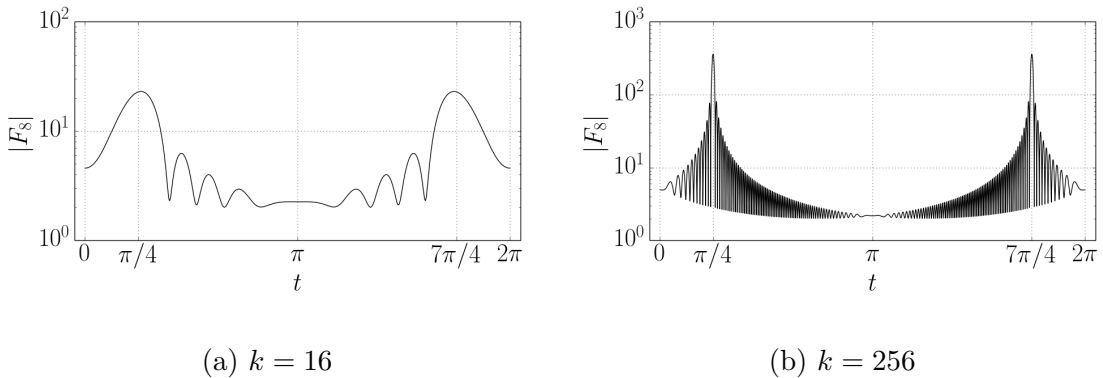


Figure 5.11: Magnitude of the far field pattern $|F_p|$ with $p = 8$ for two wave numbers $k = 16$ and $k = 256$. Scattering problem with one screen Γ_1 and incidence $\mathbf{d} = (1/\sqrt{2}, -1/\sqrt{2})$.

Another quantity of interest is the far-field pattern F . We compute a numerical approximation F_p to the far-field pattern according to [16], as

$$F_p(\hat{\mathbf{x}}) = - \int_{\Gamma} (\Psi(\mathbf{y}) + k\varphi_p(\mathbf{y})) e^{-ik\hat{\mathbf{x}} \cdot \mathbf{y}} ds(\mathbf{y}), \quad \hat{\mathbf{x}} = \frac{\mathbf{x}}{|\mathbf{x}|} \in \mathbb{S}^1, \quad (5.11)$$

where \mathbb{S}^1 denotes the unit circle.

The magnitude of the far-field pattern $|F_p|(t)$ with $p = 8$ for $t \in [0, 2\pi]$ at two values of the wave number $k = 16$ and $k = 256$ is given in Figure 5.11. The peaks corresponding to the specular reflection and geometrical shadow are clearly identifiable respectively at $t = \pi/4$ and $t = 3\pi/4$.

Again, no theoretical error estimates are available for the numerical approximation of the far field pattern F_p . However, following the proof of Theorem 6.3 in [16], we remark that for $\hat{\mathbf{x}} \in \mathbb{S}^1$, we have

$$|F(\hat{\mathbf{x}}) - F_p(\hat{\mathbf{x}})| = k |\langle e^{-ik\hat{\mathbf{x}}\cdot(\cdot)}, \varphi - \varphi_p \rangle_\Gamma|, \quad (5.12)$$

$$\leq k \|e^{-ik\hat{\mathbf{x}}\cdot(\cdot)}\|_{H_k^{1/2}(\Gamma)} \|\varphi - \varphi_p\|_{\tilde{H}_k^{-1/2}(\Gamma)}, \quad (5.13)$$

where the duality pairing $\langle \cdot, \cdot \rangle_\Gamma$ on $H^{1/2}(\Gamma) \times \tilde{H}^{-1/2}(\Gamma)$ is defined precisely in [9]. The quantity $\|e^{-ik\hat{\mathbf{x}}\cdot(\cdot)}\|_{H_k^{1/2}(\Gamma)}$ is bounded on Γ by a constant with k dependence behaving like $\mathcal{O}(\sqrt{k})$; see Lemma 4.6(i) in [16]. Again, for the far-field pattern, the previous results hint at the possibility to have exponential convergence of the numerical approximation F_p .

We approximate the infinity norm on \mathbb{S}^1 by sampling the unit circle using 50 000 points. We compute the following relative error $\tilde{r}_p[F_p]$, using the numerical approximation F_8 as the reference solution,

$$\tilde{r}_p[F_p] := \frac{\max_{\hat{\mathbf{x}} \in \mathbb{S}^1} |F_p(\hat{\mathbf{x}}) - F_8(\hat{\mathbf{x}})|}{\max_{\hat{\mathbf{x}} \in \mathbb{S}^1} |F_8(\hat{\mathbf{x}})|}. \quad (5.14)$$

The convergence plots of the error $\tilde{r}_p[F_p]$ are given in Figure 5.12. The convergence rates observed are similar to that of the convergence in the domain for the wave field u_p .

5.2 A more challenging test case

To demonstrate the capabilities of the method and its implementation in handling more difficult problems, we now present a more challenging test case taken from [16]. The test consists of $n_s = 5$ screens $\Gamma = \bigcup_{i=1}^{n_s} \Gamma_i$, as defined in (2.2) and such that

$$s_1 = 0, \quad s_2 = 2\pi, \quad s_3 = \frac{21\pi}{10}, \quad s_4 = \frac{5\pi}{2}, \quad s_5 = \frac{14\pi}{5}, \quad s_6 = \frac{7\pi}{2}, \quad (5.15a)$$

$$s_7 = 4\pi, \quad s_8 = 6\pi, \quad s_9 = \frac{61\pi}{10}, \quad s_{10} = L = 10\pi. \quad (5.15b)$$

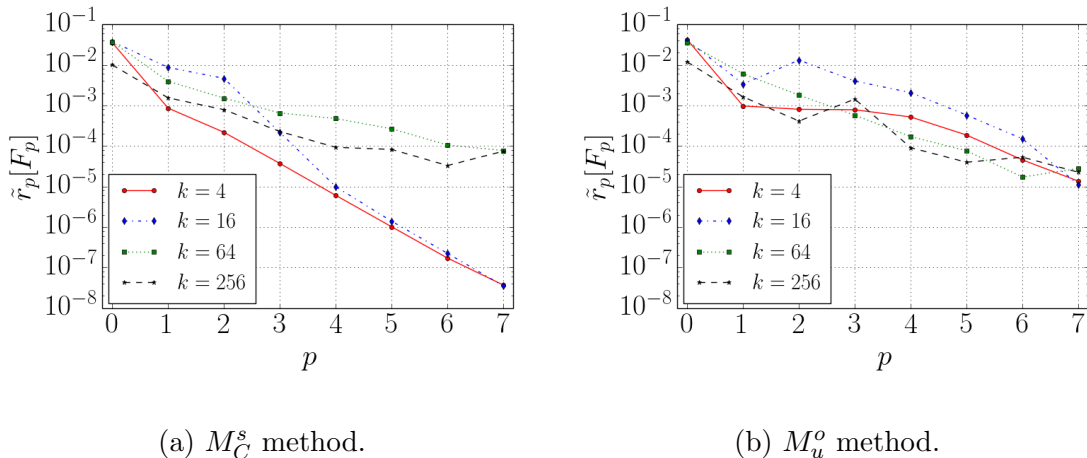


Figure 5.12: Comparison of the convergence of the relative error $\tilde{r}_p[F_p]$ with respect to the polynomial degree p for several frequencies. Scattering problem with one screen Γ_1 and with incidence $\mathbf{d} = (1/\sqrt{2}, -1/\sqrt{2})$.

We consider for this problem the 'non-grazing' incidence $\mathbf{d} = (1/\sqrt{2}, -1/\sqrt{2})$ as well as the 'grazing' incidence $\mathbf{d} = (1, 0)$. This problem is more challenging by the number of screens, the variety of the lengths and separations between the screens and the incidences considered.

The solution $|\varphi_p|$ with $p = 15$ and $c_L = 1$ on the boundary Γ for two frequencies $k = 10$ and $k = 2560$ is given in Figure 5.13. For this test, the choice $c_L = 1$ has been retained in order to limit the mesh refinement as the maximal polynomial degree is increased. Note that as a result, we are able to obtain numerical solutions for very high values of p .

The real part of the total field u is represented in Figure 5.14a for the non-grazing incidence $\mathbf{d} = (1/\sqrt{2}, -1/\sqrt{2})$ and in Figure 5.14b for the grazing incidence $\mathbf{d} = (1, 0)$, both with a wave number $k = 5$. The magnitude of the far-field pattern $|F_p|$ with $p = 15$ is represented in Figure 5.15 for the two incidences considered and for $k = 16$.

We present convergence results of the numerical solution φ_p for $p < 15$, using the numerical solution computed with $p = 15$ as a reference solution. The convergence of the relative error $\tilde{r}_p[\phi_p]$ as defined in (5.6) is given in Figure 5.16 for several frequencies and the two incidences considered. Exponential convergence is achieved again on this more challenging problem, with a convergence rate independent of the wave number.

The relative error in the domain, noted $\tilde{r}_p[u]$, is computed on the perimeter of a rectangle, noted R , with corners at $(-\pi, -\pi)$, $(11\pi, -\pi)$, $(11\pi, \pi)$, $(-\pi, \pi)$ which

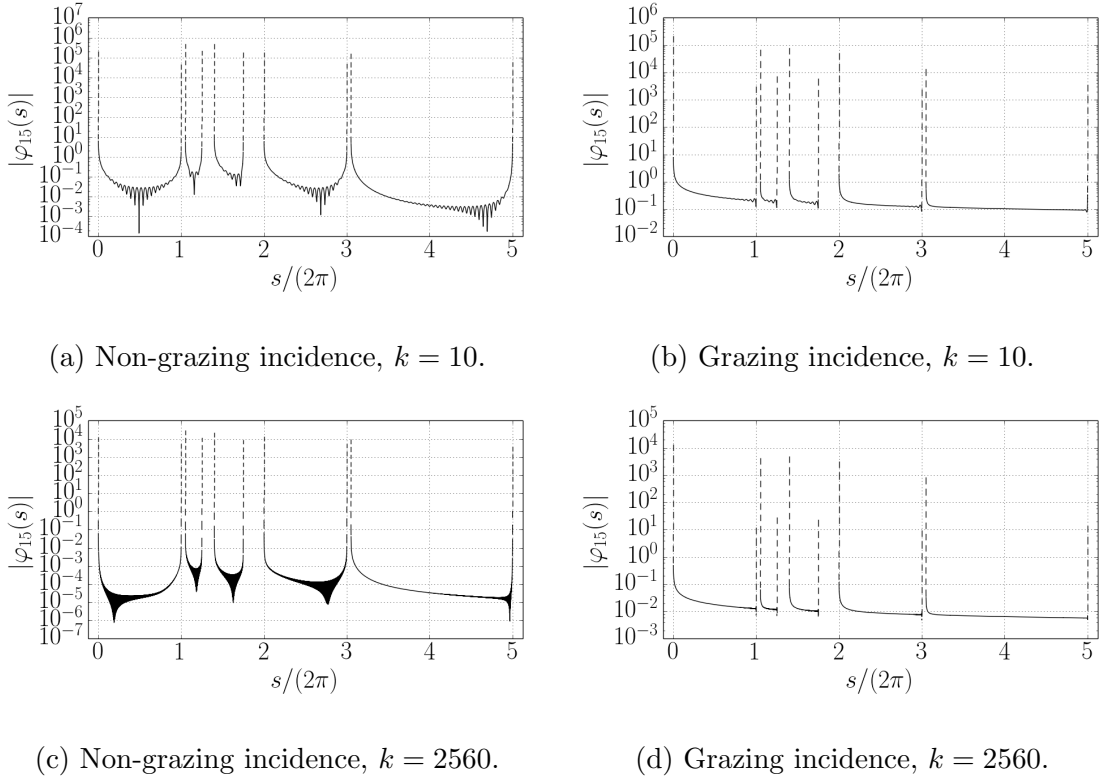
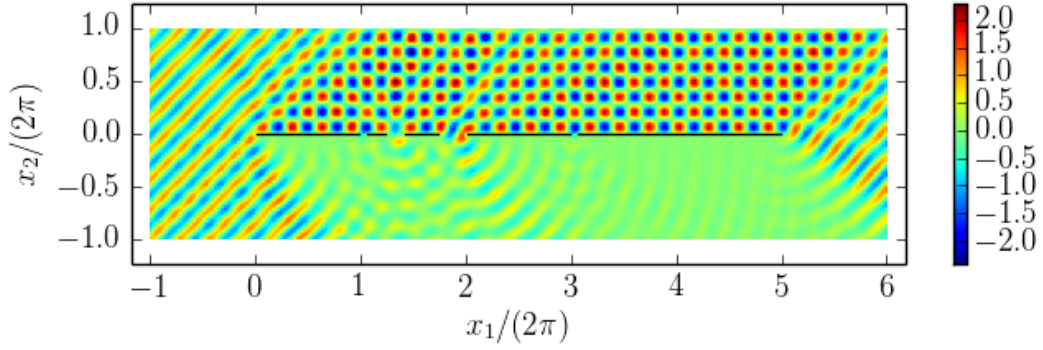


Figure 5.13: Solution $|\varphi_p|$ with $p = 15$ on the boundary Γ of the scatterer for the scattering problem with five screens, for two wave numbers $k = 10$ and $k = 2560$ and for the grazing $\mathbf{d} = (1, 0)$ and non-grazing $\mathbf{d} = (1/\sqrt{2}, -1/\sqrt{2})$ incidences.

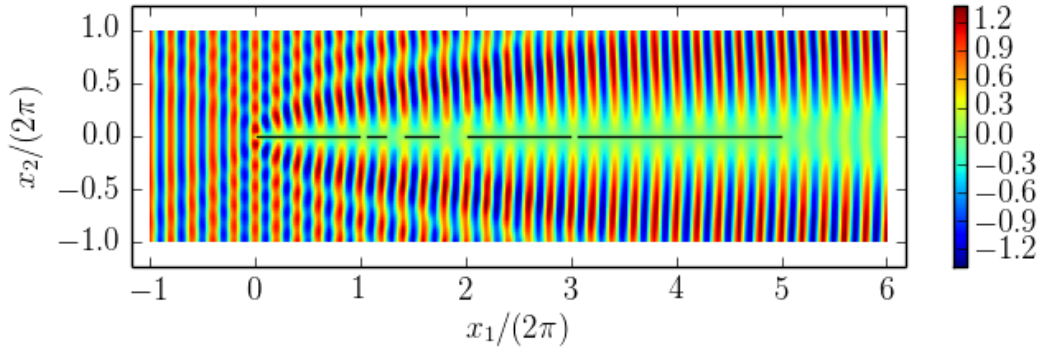
surrounds the screens, and sampled with at least 10 points per wavelength, such that

$$\tilde{r}_p[u_p] := \frac{\max_{\mathbf{x} \in R} |u_p(\mathbf{x}) - u_{15}(\mathbf{x})|}{\max_{\mathbf{x} \in R} |u_{15}(\mathbf{x})|}. \quad (5.16)$$

The reference solution used is u_p with $p = 15$. The convergence of the relative error $\tilde{r}_p[u_p]$ in the domain D is given in Figure 5.17, for several frequencies and the two incidences considered. The relative error in the far field pattern, noted $\tilde{r}_p[F_p]$ is computed according to (5.14) but using F_p with $p = 15$ as the reference solution. The convergence of the relative error in the far field pattern $\tilde{r}_p[F_p]$ is given in Figure 5.18, for several frequencies and the two incidences considered. Note that the results obtained with the M_u^o method with $p = 8$ are affected by conditioning issues. Convergence of the numerical approximations u_p and F_p is again obtained for this more challenging problem, demonstrating the robustness of the method in handling more complicated scatterer.

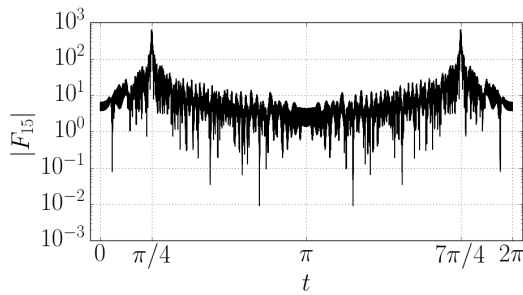


(a) Non-grazing incidence.

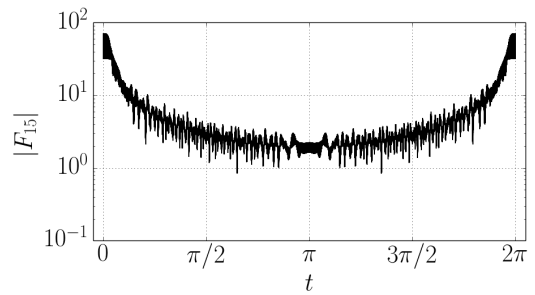


(b) Grazing incidence.

Figure 5.14: Real part of the total field $u = u^i + u^s$ in the domain D for the scattering problem with five screens, wave number $k = 5$ and for the grazing $\mathbf{d} = (1, 0)$ and non-grazing $\mathbf{d} = (1/\sqrt{2}, -1/\sqrt{2})$ incidences.

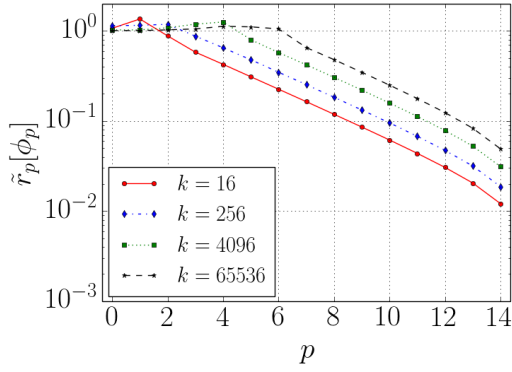


(a) Non-grazing incidence.

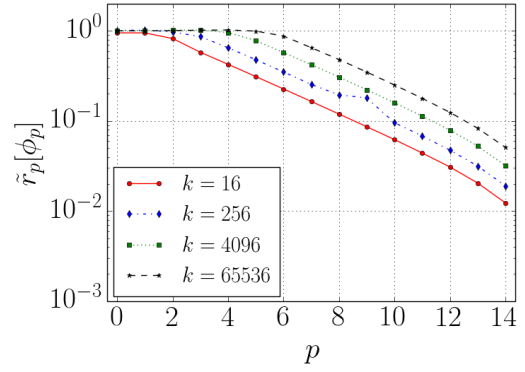


(b) Grazing incidence.

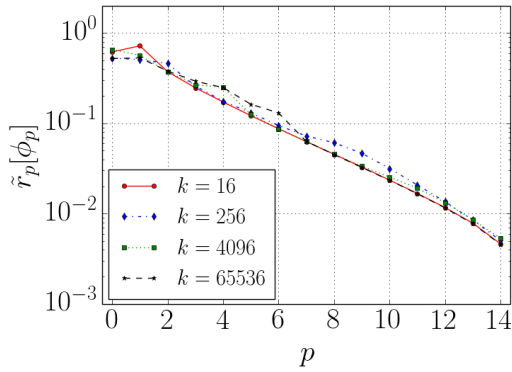
Figure 5.15: Far field pattern $|F_p|$ with $p = 15$ for the scattering problem with five screens, wave number $k = 16$ and for the grazing $\mathbf{d} = (1, 0)$ and non-grazing $\mathbf{d} = (1/\sqrt{2}, -1/\sqrt{2})$ incidences.



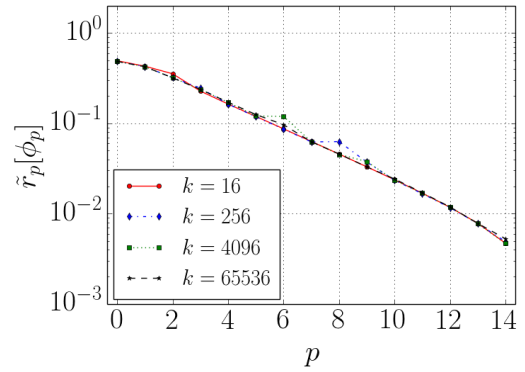
(a) M_C^s method. Non-grazing incidence.



(b) M_u^o method. Non-grazing incidence.

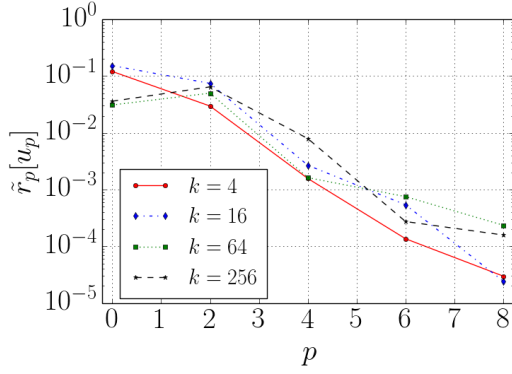


(c) M_C^s method. Grazing incidence.

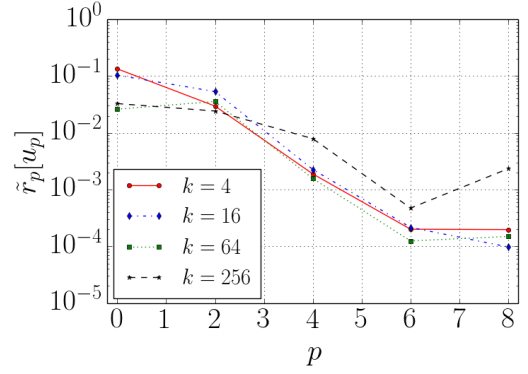


(d) M_u^o method. Grazing incidence.

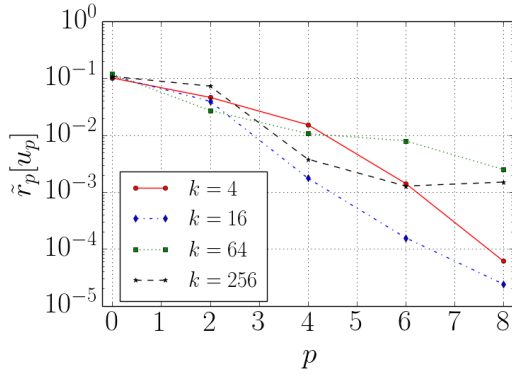
Figure 5.16: Comparison of the convergence of the relative error $\tilde{r}_p[\phi_p]$ on the boundary Γ of the scatterer with respect to the polynomial degree p and for several frequencies. Scattering problem with five screens for the grazing $\mathbf{d} = (1, 0)$ and non-grazing $\mathbf{d} = (1/\sqrt{2}, -1/\sqrt{2})$ incidences.



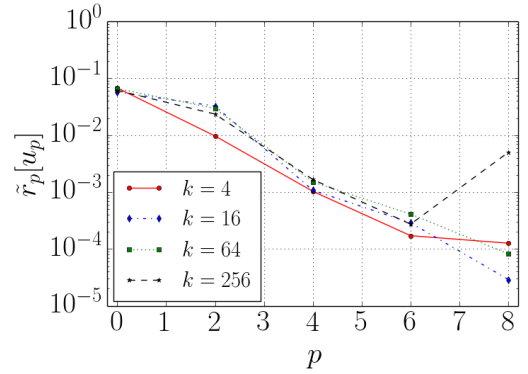
(a) M_C^s method. Non-grazing incidence.



(b) M_u^o method. Non-grazing incidence.

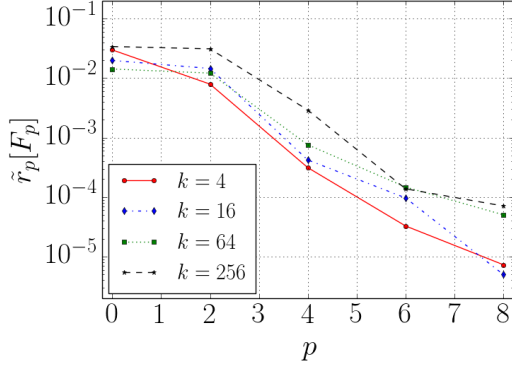


(c) M_C^s method. Grazing incidence.

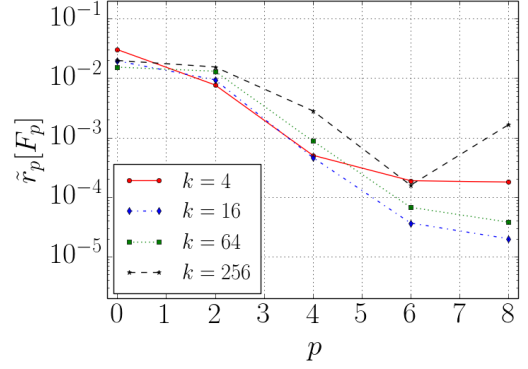


(d) M_u^o method. Grazing incidence.

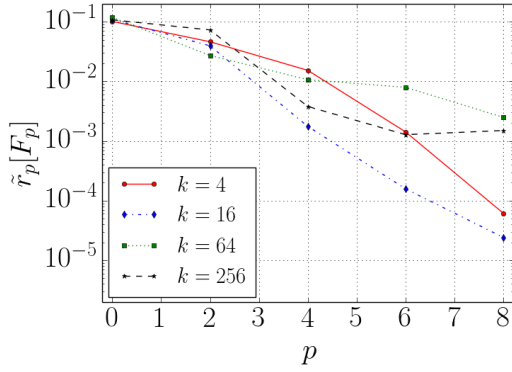
Figure 5.17: Comparison of the convergence of the relative error $\tilde{r}_p[u_p]$ in the domain of propagation D with respect to the polynomial degree p and for several frequencies. Scattering problem with five screens for the grazing $\mathbf{d} = (1, 0)$ and non-grazing $\mathbf{d} = (1/\sqrt{2}, -1/\sqrt{2})$ incidences.



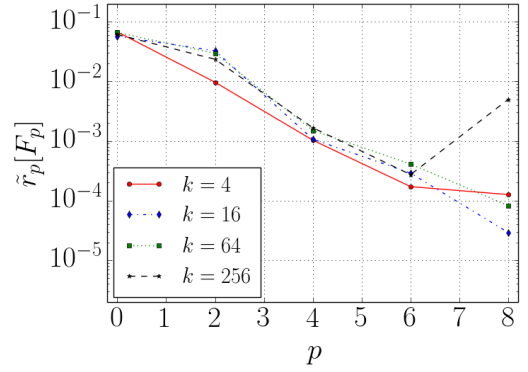
(a) M_C^s method. Non-grazing incidence.



(b) M_u^o method. Non-grazing incidence.



(c) M_C^s method. Grazing incidence.



(d) M_u^o method. Grazing incidence.

Figure 5.18: Comparison of the convergence of the relative error $\tilde{r}_p[F_p]$ for the far field pattern F_p with respect to the polynomial degree p and for several frequencies. Scattering problem with five screens for the grazing $\mathbf{d} = (1, 0)$ and non-grazing $\mathbf{d} = (1/\sqrt{2}, -1/\sqrt{2})$ incidences.

5.3 Execution time

Conventional numerical methods to solve wave scattering problems similar to the ones presented in this work have a strongly k -dependent computational cost. In particular, the number of degrees of freedom used to achieve a given accuracy typically increases at least linearly with the wave number k . On the contrary, the hybrid numerical-asymptotic approximation space used in the method we presented has the remarkable feature that the number of degrees of freedom required to achieve a given accuracy and the computational cost are essentially constant as the frequency increases.

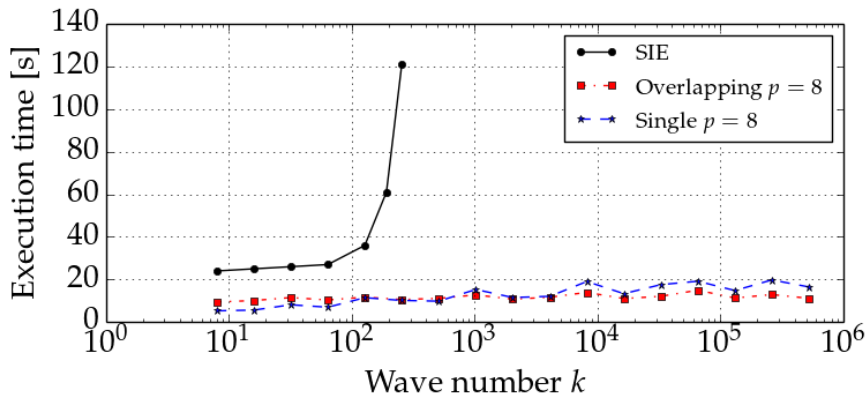


Figure 5.19: Comparison of the execution time between the `SingularIntegralEquations.jl` JULIA package (SIE), the single mesh strategy with Chebyshev collocation points, and the overlapping meshing with uniform distribution of the collocation points method. The maximum polynomial degree used for these last two methods is $p = 8$.

To illustrate this, we plot the computational time required by our two preferred methods together with the computational time required by the method implemented in the `SingularIntegralEquations.jl` JULIA package that provides our reference solution. The test case is the wave scattering problem as in Section 5.1 consisting of one single screen Γ_1 and oblique incidence $\mathbf{d} = (1/\sqrt{2}, -1/\sqrt{2})$. The results are given in Figure 5.19. The execution time used to solve the problem by the JULIA package grows like a polynomial law in the wave number k [29]. The computational cost of the overlapping meshing method with uniform allocation of the collocation points is fairly constant for the wide range of frequencies considered. The single mesh strategy with Chebyshev collocation points has a slight increase in the computational cost, due to the increase of number of degrees of freedom used for a given p , as the wave number k

increases. However the increase in computational cost is appreciably small compared to the range of frequencies considered and is bounded from above uniformly in k (as the number of degrees of freedom N is bounded from above uniformly in k).

Note importantly that the frequency-independent computational cost of the method is due to the implementation of efficient quadrature rules. Note importantly that the fact that the method has a computational cost frequency independent was made possible by the implementation of efficient quadrature rules to compute highly oscillatory integrals in a k independent fashion. The development of HNA methods at high frequencies relies therefore strongly on the availability and efficiency of such quadrature methods.

Chapter 6

Conclusions

The application of a hybrid numerical-asymptotic boundary element method for solving the boundary integral equation arising from the problem of high-frequency wave scattering by two-dimensional planar screens has been investigated. If the efficiency of such HNA BEM using Galerkin schemes is relatively well understood, both theoretically and numerically [11, 10, 17, 16], little is known on collocation approaches for such methods, with the exception of [2]. This work has mainly shown that using a collocation method can indeed be an efficient and robust strategy, provided some care is taken in its practical implementation.

Two types of HNA approximation spaces were investigated. The first one, for which a best-approximation result holds, involves two overlapping meshes to approximate the two oscillatory components of the solution. The second one relies on a single mesh, in an attempt to simplify the structure of the approximation. In both cases, the approximation space is carefully designed to minimise conditioning problems as the number of degrees of freedom N increases.

The collocation method we put into place to numerically select elements in these approximation spaces requires to choose a distribution of N collocation points on the boundary. The allocation of these points can be done in various ways. The uniform and Chebyshev distributions, locally on the mesh elements, have been considered.

In our numerical experiments, two different strategies have proved to solve efficiently the problem, namely the strategy based on an approximation space using a single mesh with a Chebyshev distribution of the collocation points, and the strategy based on an approximation space using two overlapping meshes with a uniform distribution of the collocation points.

For these two successful strategies, we numerically obtained exponential convergence of the numerical solution on the boundary as the maximum polynomial degree

p of the approximation increases. This numerical result hints at the possibility that the collocation BEM actually achieves quasi-optimality. We also show convergence of our numerical solution in the domain of propagation and in the far-field, although the convergence rate is not precisely identified.

We finally emphasise that these results were obtained with a number of degrees of freedom fairly constant with respect to the frequency of the problem. The convergence of the numerical solution on the boundary actually improves as the frequency increases. In fact the computational cost of this HNA method is (almost) frequency-independent. This result was made possible by the implementation of efficient highly oscillatory numerical quadrature. The well-known behaviour of the integrands in the integrals considered greatly simplified the construction of dedicated numerical integrators.

In future work, the numerical instabilities observed with the approximation space based on two overlapping meshes with a Chebyshev distribution of the collocation points could be further investigated. We also note that we implicitly assumed that the number of collocation is equal to the number of degrees of freedom N . However nothing prevents us from considering a higher number of collocation points and the over-determined systems associated. Other possibilities of extensions include Neumann or Robin problems, which are often of high interest for acoustic applications, and other formulations of the boundary integral equations.

References

- [1] NIST Digital Library of Mathematical Functions. <http://dlmf.nist.gov/>, Release 1.0.9 of 2014-08-29. Online companion to [26].
- [2] S. ARDEN, S. N. CHANDLER-WILDE, AND S. LANGDON. A collocation method for high-frequency scattering by convex polygons. *Journal of Computational and Applied Mathematics*, **204**:334–343, 2007.
- [3] A. ASHEIM AND D. HUYBRECHS. Local solutions to high-frequency 2d scattering problems. *Journal of Computational Physics*, **229**:5357–5372, 2010.
- [4] K.E. ATKINSON. The numerical solution of integral equations of the second kind. 1997.
- [5] V. A. BOROVIKOV AND B. YE. KINBER. *Geometrical Theory of Diffraction*. IEE electromagnetic waves series. Institution of Electrical Engineers, 1994.
- [6] O. P. BRUNO AND S. K. LINTNER. Second-kind integral solvers for TE and TM problems of diffraction by open arcs. *Radio Science*, **47**, 2012. RS6006.
- [7] G. CHANDLER AND I. G. GRAHAM. Product integration-collocation methods for non-compact integral operator equations. *Mathematics of Computation*, **50**:125–138, 1988.
- [8] S. N. CHANDLER-WILDE, I. G. GRAHAM, S. LANGDON, AND E. A. SPENCE. Numerical-asymptotic boundary integral methods in high-frequency scattering. *Acta Numerica*, pages 89–305, 2012.
- [9] S. N. CHANDLER-WILDE AND D. P. HEWETT. Wavenumber-explicit continuity and coercivity estimates in acoustic scattering by planar screens. *Integral Equations and Operator Theory*, **83**(3):423–449, 2015.

- [10] S. N. CHANDLER-WILDE, D. P. HEWETT, S. LANGDON, AND A. TWIGGER. A high frequency boundary element method for scattering by a class of nonconvex obstacles. *Numerische Mathematik*, **129**(4):647–689, 2014.
- [11] S. N. CHANDLER-WILDE AND S. LANGDON. A Galerkin boundary element method for high frequency scattering by convex polygons. *SIAM Journal of Numerical Analysis*, **45**:610–640, 2007.
- [12] S. N. CHANDLER-WILDE, S. LANGDON, AND L. RITTER. A high-wavenumber boundary element method for an acoustic scattering problem. *Philosophical Transactions of the Royal Society A*, (362):647–671, 2004.
- [13] K. CHEN AND S. AMINI. Numerical analysis of boundary integral solution of the Helmholtz equation in domains with non-smooth boundaries. *IMA Journal of Numerical Analysis*, **13**:43–66, 1993.
- [14] M. COSTABEL AND E. STEPHAN. On the convergence of collocation methods for boundary integrals equations on polygons. *Mathematics of Computation*, **49**:461–478, 1987.
- [15] A. GLASER, X. LIU, AND V. ROKHLIN. A fast algorithm for the calculation of the roots of special functions. *SIAM Journal on Scientific Computing*, **29**:1420–1438, 2007.
- [16] D. P. HEWETT, S. LANGDON, AND S. N. CHANDLER-WILDE. A frequency-independent boundary element method for scattering by two-dimensional screens and apertures. *IMA Journal of Numerical Analysis Advance Access*, 2014.
- [17] D. P. HEWETT, S. LANGDON, AND MELENK J. M. A high frequency hp boundary element method for scattering by convex polygons. *SIAM Journal of Numerical Analysis*, **51**(1):629–653, 2013.
- [18] D. HUYBRECHS AND S. OLVER. *Highly Oscillatory Quadrature*. Highly Oscillatory Problems. Cambridge University Press, 2009.
- [19] D. HUYBRECHS AND S. VANDEWALLE. On the evaluation of highly oscillatory integrals by analytic continuation. *SIAM Journal of Numerical Analysis*, **44**(3):1026–1048, 2006.
- [20] A. ISERLES AND S. NORSETT. On quadrature methods for highly oscillatory integrals and their implementation. *BIT*, **44**:755–772, 2005.

- [21] T. KIM. *Asymptotic and numerical methods for high-frequency scattering problems*. PhD thesis, University of Bath, 2012.
- [22] R. KRESS. *Linear Integral Equations*. Applied mathematical sciences. Springer, New York, 2010.
- [23] W. MCLEAN. *Strongly Elliptic Systems and Boundary Integral Equations*. CUP, 2000.
- [24] J. M. MELENK. On the convergence of Filon quadrature. *Journal of Computational and Applied Mathematics*, **234**:1692–1701, 2010.
- [25] E.J. NYSTRÖM. Über Die Praktische Auflösung von Integralgleichungen mit Anwendungen auf Randwertaufgaben. *Acta Mathematica*, **54**(1):185–204, 1930.
- [26] F. W. J. OLVER, D. W. LOZIER, R. F. BOISVERT, AND C. W. CLARK, editors. *NIST Handbook of Mathematical Functions*. Cambridge University Press, New York, NY, 2010. Print companion to [1].
- [27] P. PETRAS. On the computation of the Gauss-Legendre quadrature form with a given precision. *Journal of Computational and Applied Mathematics*, **112**:253–267, 1999.
- [28] C. SCHWAB. *p- and hp- Finite Element Methods*. Numerical Mathematics and Scientific Computation. Clarendon Press, 1998.
- [29] M. SLEVINSKY AND S. OLVER. A fast and well-conditioned spectral method for singular integral equations. In preparation, 2015.
- [30] I. H. SLOAN. Error analysis of boundary integral methods. *Acta Numerica*, pages 287–339, 1991.
- [31] L. N. TREFETHEN. *Approximation Theory and Approximation Practice*. SIAM, 2013.
- [32] I. G. GRAHAM V. DOMINGUEZ AND V. P. SMYSHLYAEV. A hybrid numerical-asymptotic boundary integral method for high-frequency acoustic scattering. *Numerische Mathematik*, **106**(3):471–510, 2007.